JGS
Journal of the Geological Society

Research article

https://doi.org/10.1144/jgs2024-146 | Vol. 182 | 2025 | jgs2024-146

Climatic and tectonic controls on ferroan dolomite formation: insights into Early Miocene anoxia in the Mediterranean Sea (il-Blata, Malta)

Ray Zammit[1,2*], Daniel A. Petrash[3] and Or M. Bialik[4,5]

[1] School of Earth and Environmental Sciences, Cardiff University, Cardiff CF10 3AT, UK
[2] Department of Mathematics & Science Education, Faculty of Education, The University of Malta, Msida MSD 2080, Malta
[3] Department of Environmental Geochemistry and Biogeochemistry, Czech Geological Survey, Prague, Czech Republic
[4] Institut für Geologie und Paläontologie, University of Münster, 48149 Münster, Germany
[5] Dr Moses Strauss Department of Marine Geosciences, Leon H. Charney School of Marine Sciences, University of Haifa, Haifa, Israel

RZ, 0000-0002-8629-3793; DAP, 0000-0001-5039-0543; OMB, 0000-0003-1915-7297
* Correspondence: zammitr2@cardiff.ac.uk; raymond.zammit@um.edu.mt

Abstract: Records from the Miocene il-Blata section in Malta offer insights into the depositional environments of the Central Mediterranean following an Early Miocene restriction of the Mesopotamian Seaway (*c.* 20 Ma). Inorganic and organic stable carbon isotope values suggest relatively steady depositional environments, whereas authigenic iron dolomite abundances exhibiting substantial $\delta^{18}O$ and $\delta^{13}C$ variations at a sequence scale indicate dynamic sedimentation conditions leading to differential diagenesis. Petrographically, the dolomitic levels exhibit matrix-selective dolomitization, occasional silicification and phosphatization, and textural indicators pointing to subsurface microbial influences. These features collectively point to complex shallow burial diagenesis. In addition, the presence of framboidal pyrite and gypsum infilling foraminiferal chambers, along with the absence of large planktonic foraminifera, suggests the development of palaeoenvironmental stress imposed by a density-stratified water column affecting the pore waters. Towards the top of the studied succession, a shift from organic to siliceous deposits reflects water column perturbations possibly linked to changes in oceanic circulation associated with a temporary re-opening of the Mesopotamian Seaway. This study not only underscores the hydrochemical controls exerted by North African terrigenous fluxes over the Mediterranean, but also highlights the intricate interplay between shifting depositional environments and shallow burial diagenetic processes in shaping the geochemical and textural fabrics of authigenic mineral assemblages.

Supplementary material: Tables containing geochemical data, SEM images and EDS records from selected samples from the Early Miocene il-Blata section (Malta) are available at https://doi.org/10.6084/m9.figshare.c.7618306

Received 25 July 2024; **revised** 19 December 2024; **accepted** 2 January 2025

Autochthonous biogenic sedimentation in pelagic and hemipelagic realms is considered to be predominantly a mixture of two modes: (1) the slow background rain of biogenic debris from the sea surface; and (2) rapid solute influxes associated with blooms in biological productivity (Hüneke and Henrich 2011). Biogenic productivity is dependent on the availability of nutrients, notably nitrogen, phosphate and silica, as well as micronutrients such as iron, which is considered to be the main bio-limiting nutrient in marine systems (Emerson 2016; Jiang *et al.* 2023). Iron fluxes into open marine settings can be from varying combinations of continental runoff, aeolian input, the resuspension of shallow sediments, ice-rafted debris, extraterrestrial sources, subaerial and submarine volcanism, and exhalative hydrothermal inputs (Boyd and Ellwood 2010; Emerson 2016). The provenance of the iron entering a marine system can vary, with certain fluxes becoming more important than others at different sites and between different ocean basins. It has been shown that some of the modes of ancient oceanic iron delivery affecting palaeoproductivity may be controlled by astronomical cycles (Auer *et al.* 2016; Kocken *et al.* 2019; Lyu *et al.* 2023). In more recent geological history, Holocene glacial–interglacial changes in atmospheric carbon dioxide oscillations have also been linked to the availability of iron for surface ocean productivity, with iron being a key component for phytoplankton-controlled feedbacks in the carbon cycle (Martin 1990; Watson *et al.* 2000).

Neogene and Holocene marine sediments contain significant amounts of dolomite [$CaMg(CO_3)_2$] and related rhombohedral phases comprising the dolomite–ankerite series (Petrash *et al.* 2017; Liu *et al.* 2024). Ankerite [$Ca, Fe(CO_3)_2$] *sensu stricto* is a carbonate mineral in which iron completely replaces magnesium in the rhombohedral dolomite structure, although such a complete replacement has never been observed in nature. By contrast, kutnohorite [$Ca, Mn(CO_3)_2$] demonstrates that magnesium can be fully replaced by manganese (Bridges *et al.* 2014). Intermediary minerals with the general formula [$Ca(Fe, Mg, Mn)(CO_3)_2$], in which the divalent cations are incorporated in the rhombohedral $\bar{R}3$ structure, do exist and are named according to the cation ratio (Bridges *et al.* 2014; Liu *et al.* 2024). In this scheme, the dolomite–ankerite series represents a compositional continuum between pure dolomite with a molar ratio of $Mg/(Mg + Fe) = 1$ and pure ankerite, which has $Mg/(Mg + Fe) = 0$. The intermediate compositions are termed iron dolomite [$(Mg/(Mg + Fe) \geq 0.5$] or magnesium ankerite [$(Mg/(Mg + Fe) < 0.5$] (Bridges *et al.* 2014). This series reflects the geochemical conditions of precipitation, with all members maintaining the $\bar{R}3$ symmetry.

The formation of iron-bearing dolomite is directly influenced by the evolving composition of intermediate diagenetic fluids (Woods and Garrels 1992; Böttcher and Dietzel 2011), with the diagenetic realm defined as burial depths from hundreds of metres to *c.* 2 km (*T*

<100°C) (Immenhauser 2022). For example, the iron content of dolomite in the Monterey Formation, which registers maximum diagenetic temperatures of *c.* 45–50°C, achieved at burial depths ≤750 m (Isaacs 1982; Eichhubl and Boles 2000; Bradbury *et al.* 2015), appears to increase in zones exhibiting large fluxes of terrigenous material (Burns and Baker 1987). The reasons for this are (1) the rapid burial of sediment quickly buries reactive iron, making it available for incorporation into dolomite formed prior to the onset of sulfate reduction and (2) high sedimentation rates are associated with large fluxes of terrigenous material, which is the main source of iron to a basin (Burns and Baker 1987).

Reactive iron-bearing lithologies are usually associated with siliceous deposits (e.g. cherts), with a strong control exerted by inputs of silica from continental weathering (Maliva *et al.* 2005). Chert nodules are generally thought to form as a series of replacement and void-filling processes within sediments. The exact implications in terms of the origin and the palaeoceanographic and climatic significance of these deposits remain uncertain (Madsen and Stemmerik 2010). It has been suggested that the removal of silica from seawater and its eventual incorporation into sediments is driven by the redox cycling of iron (Li *et al.* 2022). In this model, silicon is precipitated from seawater in conjunction with iron in the form of Fe^{III}–Si gels. These gels are disassociated in anoxic sediments, releasing the silicon, which is preserved in sediments (Li *et al.* 2022). This supports the link between iron redox cycling and chert formation.

In (sub)polar regions, the supply of iron through aeolian inputs is well characterized because only a few major rivers are present. The situation in subtropical and tropical regions, however, is more complex due to the presence of significant river systems. In these regions, the intricate interplay of riverine and aeolian inputs opens up the possibility of transient, localized excesses of oceanic iron, the effects of which in the sediment authigenic response are unclear (Boyd and Ellwood 2010; Jickells and Moore 2015).

The southern Mediterranean is an ideal place to investigate the effects of iron availability on bioproductivity due to its proximity to the North African land mass, a large source of continental-derived solutes and nutrients, and its enclosed nature (Fig. 1). Moreover, the distant influence of runoff and dust from the relatively arid North African margin allows for a degree of control and differentiation between these sources. It has previously been reported that diagenetic ankerite occurs within the Miocene Globigerina Limestone Formation on the Central Mediterranean archipelago of Malta (John *et al.* 2003). More recent characterization of the Globigerina Limestone Formation has revealed the presence of Early Miocene organic-rich carbonate mudstones and overlying chert-bearing deposits (Zammit *et al.* 2022). The shift from shallow marine phosphorite-bearing limestones to these organic-rich cherty deposits may represent a response to the temporary closure of the Mesopotamian gateway and the ensuing perturbations in Mediterranean circulation and increased hydroclimatic activity over western North Africa at *c.* 20 Ma (Zammit *et al.* 2022). These il-Blata deposits therefore offer an opportunity to investigate the influence of a changing hydroclimate over North Africa and the restriction of the Mediterranean basin on depositional systems in the Central Mediterranean.

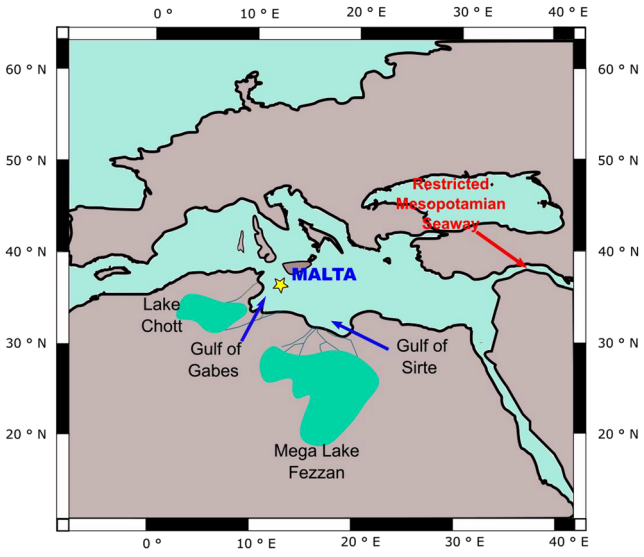

Fig. 1. The Mesopotamian Seaway connecting the Mediterranean Sea with the Indian Ocean became severely restricted at *c.* 20 Ma due to tectonic movements of the African and Arabian plates (Bialik *et al.* 2019) This configuration favoured intensified weather over the Atlantic Ocean, resulting in a wetter western Sahara region and a high siliciclastic input into the Central Mediterranean via continental runoff. The mixed carbonate–siliciclastic deposits of Malta (denoted by a star) hold a record of these events.

For this purpose, we elucidated the water column processes associated with a variability in nutrient fluxes that could exert an authigenic response in depositional systems. We hypothesized that changes in solute delivery (carrying oxides, silica and phosphorus) significantly impacted mineral saturation states and dolomite precipitation rates in a way that induced fabric-preserving dolomitization. To address these hypotheses, we posed the following research questions: (1) what are the characteristics and stratigraphic location of diagenetic iron-bearing dolomites in the Maltese outcrops and how is their formation associated with Mediterranean palaeoenvironments driven by the North African hydroclimate and changes in ocean circulation; and (2) which water column processes can explain the shift from organic facies to cherty facies in the il-Blata section and how do these diagenetic processes relate to the broader palaeoenvironments influenced by the North African hydroclimate and changes in ocean circulation?

Geological setting and research context

The Mediterranean Sea (Fig. 1) is considered to be a natural laboratory in which to investigate closely coupled depositional processes driven by tectonic and climatic factors. Its hypersensitivity to these forcing factors is reflected in changes in its geochemistry, sedimentology and stratigraphy, as recorded by fossil variability and depositional cyclicity (Meijer 2021; Reich *et al.* 2022). Related changes in the water column conditions led to the preservation of a range of sedimentary rocks, from evaporites to organic-rich pelagic sediments (Rutten *et al.* 1999; Haq *et al.* 2020; Roveri *et al.* 2020; Meijer 2021; Casanova-Arenillas *et al.* 2022). The dynamic tectono-climatic evolution of the Mediterranean basin throughout the Miocene has also led to an incomplete record. This is particularly problematic during the Early Miocene, as demonstrated by the fact that a Global Boundary Stratotype Section and Point (GSSP) has never been established for either the base-Burdigalian nor the base-Langhian (Gradstein *et al.* 2020). Several regional unconformities have also been reported across the basin in sections of Mid-Miocene age (Eaton and Robertson 1993; Cipollari and Cosentino 1995). The almost complete desiccation of the basin during the Messinian salinity crisis at the end of the Miocene also lead to gaps in the stratigraphic record of the region (Haq *et al.* 2020).

Large-scale tectonic changes in the Mediterranean occurred during the Miocene (23–5.6 Ma) (Rögl 1999), with the formation of a basin in a form that closely resembles the present day, mostly enclosed, sea occurring at *c.* 14 Ma. The water flow from the Indian Ocean through the Mesopotamian Seaway was then completely closed off (Mesopotamian Seaway Restriction event number 2,

MSR-2) (Bialik *et al.* 2019; Zammit *et al.* 2022). The full extent of oceanographic and environmental changes resulting from the transition from the long-standing (*c.* 100 Ma; Barron and Peterson 1989), low-latitude halothermal circulation to a strong thermohaline system has not been fully revealed and requires detailed investigation. An enclosed configuration would have promoted the generation of oxygen minimum zones in the Eastern Basin, as evidenced by the existence of laminated, dark-coloured, sulfur-rich muds, often referred to as sapropels (Rohling 1994). Sapropel deposition in the Eastern Mediterranean reflects the hydroclimate and associated fertilization of surface waters and variability in the activity of the Nile influx to the basin (Rohling 1994; Rohling *et al.* 2015).

Mediterranean sapropels seem to have occurred almost periodically since 13.5 Ma, mostly within the Eastern Basin (Rohling *et al.* 2015). Recent work has revealed records for earlier sapropelic events (*c.* 16 Ma), as identified from sedimentary deposits in Cyprus (Taylforth *et al.* 2014; Bialik *et al.* 2022). There is also evidence for Mediterranean sapropels occurring within the Western Basin, where they are sometimes referred to as organic-rich layers (Anastasakis and Stanley 1984; Incarbona and Sprovieri 2020; Pérez-Asensio *et al.* 2020). These western organic-rich layers from Plio-Pleistocene facies exhibit plausible temporal correlation with the eastern sapropels. However, there are important exceptions, suggesting that different mechanisms may have been at play during the development of low-oxygen conditions prone to sapropel deposition (Rohling *et al.* 2015). The abundant organic matter in the sapropels can be partially degraded diagenetically, resulting in the formation of authigenic carbonates (Thomson *et al.* 2004; Leonova *et al.* 2019).

Based solely on X-ray diffraction analyses of the d_{104} distance in iron-rich diagenetic carbonates, John *et al.* (2003) identified ankerite in the Oligo-Miocene Globigerina Limestone Formation outcropping in Malta. Their interpretation is that the sedimentary processes linked to these phases and the stratigraphic clay mineral variability on the Maltese Islands were controlled by now-extinct North African drainage networks. More recent work has refined the age model for the Globigerina Limestone Formation and has revealed the presence of high-sulfur, organic-rich laminated beds occurring within the Early Miocene Middle Globigerina Limestone Member (Zammit *et al.* 2022). These thinly bedded mudstones are conformably capped by cherty mudstones that can be roughly correlated with siliceous-bearing rock formations occurring over wide areas of North Africa (Riahi *et al.* 2015; Ben Yahia *et al.* 2019).

Best exposed in the il-Blata outcrop (35° 54′ 00.6″ N, 14° 19′ 52.2″ E), these mudstones also host the geochemical record of an Early Miocene restriction episode of the Mesopotamian gateway into the Eastern Mediterranean (Mesopotamian Seaway Restriction event number 1, MSR-1) at *c.* 20 Ma (Bialik *et al.* 2019; Zammit *et al.* 2022). The il-Blata mudstone sequences are also roughly time-correlated with the intermittent activity of the Fezzan mega-lake system in North Africa (Fig. 1) (Hounslow *et al.* 2017; Drake *et al.* 2022). Other mega-lake systems, such as the Chott system, are known from more recent geological history, but there is scant evidence of their existence during the Miocene because the sedimentological evidence is obscured by sand dunes and aeolian processes (Drake *et al.* 2011, 2022).

Using known models that compare the effects on the low-latitude circulation due to the closure of the Mesopotamian Seaway, it has previously been proposed that land–ocean interactions over western North Africa would have been intensified following the closure of the seaway (de la Vara and Meijer 2016; Bialik *et al.* 2019). It can be reasonably assumed that such an intensification in land–ocean interactions resulted in increased continental runoff into the Central Mediterranean. This mechanism has been used to explain the shift from low-productivity, phosphorite-bearing marine limestones to the high sedimentation rate mixed carbonate–siliciclastic depositional system containing organic-rich layers found at the il-Blata outcrop in Malta (Zammit *et al.* 2022). Considering the presence of diagenetically altered limestones, organic-rich mudstone facies and close temporal association of the seaway restriction, it is instructive to consider which palaeoenvironmental changes in the water column were recorded in the shallow sediments of the Central Mediterranean at the time. In this context, the Maltese il-Blata outcrop is ideally placed, both temporally and geographically, to assess these phenomena and add to the growing knowledge related to iron-bearing minerals, chert nodule formation and diagenesis induced through continent-to-ocean dynamics and the regional palaeoceanography of the Early Miocene.

Methods

Outcrop sampling

More than 100 samples were collected during field excursions at the il-Blata outcrop along the southern coast of the island of Malta. These samples were obtained from the Globigerina Limestone Formation, in particular from the highly weathered Lower Globigerina Limestone Member and the overlying base level of the Middle Globigerina Limestone Member. This outcrop has been previously divided into two depositional intervals based on the coarseness of the lithology at outcrop (Zammit *et al.* 2022). Depositional Interval 1 has been divided into three sedimentary packages (I–III) and Depositional Interval 2 into four packages (IV–VII) (Fig. 2). This study examines fine-grained sequences from Depositional Interval 2, representing a transition from marine limestones in Interval 1 to mixed marine-terrestrial deposits, reflecting Early Miocene hydroclimatic changes (Zammit *et al.* 2022).

Mineralogy and geochemistry

Mineral content analyses were carried out on selected samples using a Rigaku MiniFlex 600 benchtop X-ray diffractometer (30 kV/10 mA at 0.05° increments from 3° to 70°) using Rigaku PDXL software. The total carbonate content of the bulk rock was measured using a digital calcimeter (Zammit *et al.* 2022). Semi-quantitative major element abundances were measured by X-ray fluorescence spectrometry on a total of 114 samples from the il-Blata section using an Olympus Delta Innov-X XRF gun (Zammit *et al.* 2022). From these samples, a subset of 57 samples pertaining to Depositional Interval 2 are used here. The ratios of iron, phosphorus and sulfur to the main components of the sediment [Fe/(Ca + Si + Al), P/(Ca + Si + Al) and S/(Ca + Si + Al)] were considered. The relationships among these elemental ratios were used to roughly assess the oxygenation states of the sediment at the time of deposition because the iron in anoxic sediments tends to be incorporated authigenically into sulfur-bearing phases (e.g. gregite, mackinawite or pyrite), whereas iron oxides (e.g. goethite or lepidocrocite) are major sinks for phosphorus. The detailed methods and all bulk carbonate and elemental data have been reported previously by Zammit *et al.* (2022).

A total of five representative samples (MG-55, MG-57, MG-81, MG-91 and MC-05) (Fig. 2) were analysed for both total inorganic carbon (TIC) and total organic carbon (TOC). The TIC was determined using an Eltra CS500 infrared carbon and sulfur analyser. Carbonate CO_2 was determined using a Coulomat 7012 Strohlein instrument with decomposition temperatures of 1350–1450°C and a sample weight of 50–200 mg for carbon concentrations ranging from 0.01 to 95.0%. The absorption of released CO_2 gas was measured in the infrared range. The TOC-measuring device was calibrated using an

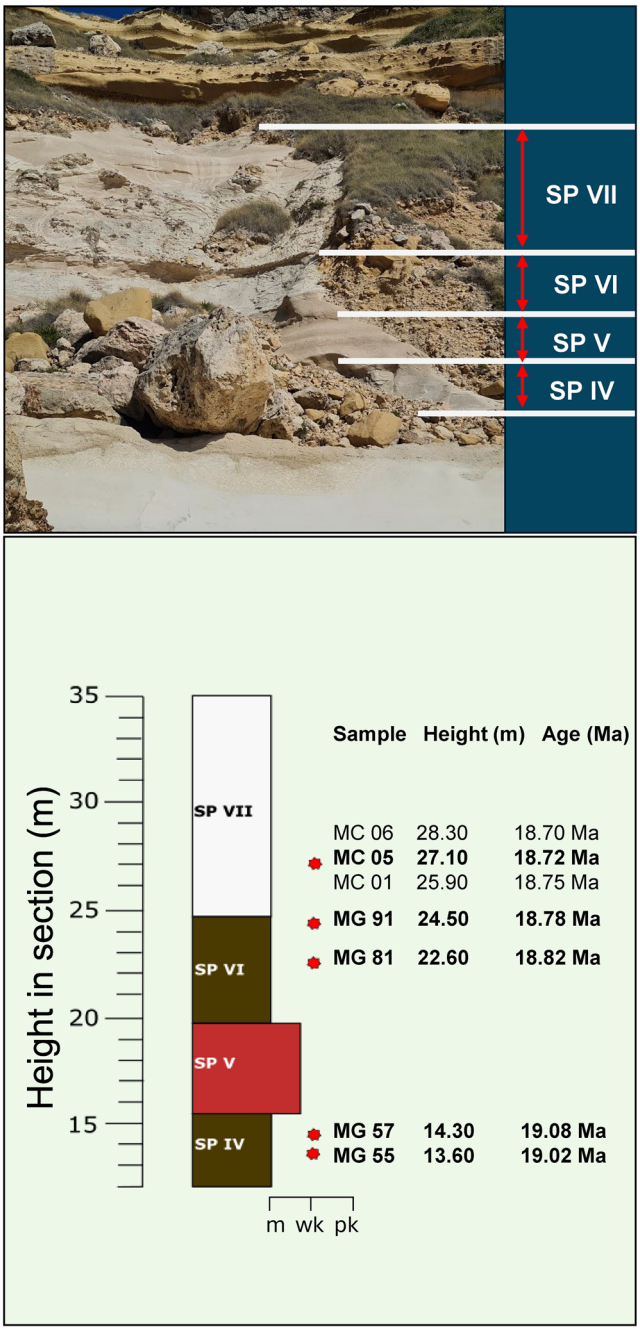

Fig. 2. The il-Blata section on the Central Mediterranean island of Malta hosts organic-rich facies superimposed by chert-rich carbonate facies of Early Miocene age. Five representative samples were selected from the organic-rich (SP IV and SP VI) and chert-rich (SP VII) packages. The ages were obtained via the $^{87}Sr/^{86}Sr$ isotope system (Zammit *et al.* 2022).

in-house reference material before initiating the analysis and its operational settings were adjusted as per the manufacturer's guidelines. The determination has an accuracy of ±3% of the reported value.

The carbon and oxygen isotope ratios of the carbonate phases were determined following the removal of organic carbon by hydrogen peroxide. The $\delta^{13}C$ and $\delta^{18}O$ values for calcite were obtained by first digesting the samples at room temperature with 100% phosphoric acid following the method of McCrea (1950). To obtain the same stable isotope records for dolomite, the samples were decalcified by treatment with 10% HCl for 20 minutes and then thoroughly rinsed five times with deionized water. The residual fraction was subsequently digested at 100°C with 100% phosphoric acid. The CO_2 released from each phase was separately analysed for $\delta^{13}C$ and $\delta^{18}O$ values using a Thermo Fisher Scientific DELTA V mass spectrometer coupled with a Fisons EA-1108 elemental analyser and a ConFlo IV reference gas interface. The isotope ratios are reported in δ notation (‰) relative to Vienna PeeDee Belemnite standard using the equation $\delta(\text{Sample}) = [(R_{sample}/R_{standard})-1] \times 10^3$, where R represents the $^{18}O/^{16}O$ or $^{13}C/^{11}C$ ratio. The acid fractionation factors used were 1.00908 for CO_2 derived from carbonates in the (Ca, Mg, Fe)(CO_3) system (Rosenbaum and Sheppard 1986) and 1.01025 for calcite (Friedman and O'Neil 1977). The in-house long-term reproducibility for $\delta^{13}C$ and $\delta^{18}O$ measurements (2σ confidence precision level) is based on combined measurements of the IAEA NBS-18 and in-house standards (Carrara Marble) and is better than ±0.1‰

Petrographic analysis

Based on the initial field evaluations and geochemical analyses, we selected four representative samples (MG-55, MG-91, MC-01 and MC-06) from Depositional Interval 2 (Zammit *et al.* 2022) of the il-Blata Section (Fig. 2). Samples MG-55 (SP IV) and MG-91 (SP VI) were obtained from fine-grained carbonate mudstone sequences, whereas MC-01 (SP VII) and MC-06 (SP VII) were from cream-coloured, fine-grained siliceous carbonate sequences rich in chert nodules (Zammit *et al.* 2022). The samples were selected to represent the evolving stratigraphy of the section. These samples underwent in-depth petrographic analysis supported by scanning electron microscopy (SEM) coupled with energy-dispersive spectrometry (EDS). A Tescan MIRA3 GMU scanning electron microscope combined with an Oxford Instruments Nordlys Nano energy-dispersive X-ray spectrometer were used. Freshly broken and polished thick sections were used for the analyses.

Results

Lithology

The bedsets considered here are divided into four sedimentary packages (SPs) on the basis of lithology (Zammit *et al.* 2022) (Fig. 2). SP IV consists of organic-rich, very thinly bedded calcareous marls containing *c.* 60% carbonate (Fig. 3a); these beds are capped by the SP V carbonates. SP V is composed of thin- to medium-bedded mudstone/wackestone facies. Within this package, phosphatic pebble horizons containing small (*c.* 1 cm) pebbles of apparent allochthonous origin are embedded in the limestone (Fig. 3b). This sedimentary package is similar to the underlying marine carbonates described in SP III of Depositional Interval 1 (Zammit *et al.* 2022) with a carbonate content of *c.* 70% and signs of bioturbation. SP VI is similar to SP IV, but is more finely laminated (Fig. 3c, d) with no sign of any bioturbation; the transition from SP V to SP VI is conformable (Fig. 3c). The finely laminated beds pertaining to SP VI alternate at the millimetre scale between very dark and lighter layers (Fig. 3d). The uppermost part of the bedsets considered here (SP VII) consists of siliceous limestones with large cherty nodules in distinct horizons (Fig. 3e–g). Its carbonate content is relatively low (*c.* 30%) and the package conformably overlies the dark layers of SP VI with a swift colour change to creamy white marls (Fig. 3f) and the incidence of cherty nodules of various sizes (Fig. 3e–g).

Elemental, mineral and isotopic compositions

The carbonate content tends to be generally high within SP IV to SP VI, with values varying between 60 and 70% by weight, although with a notable low (54%) occurring towards the base of the organic-rich SP VI. There is a trend towards low carbonate values within SP VI and a significant decrease in total carbonate in the cherty SP VII (Fig. 4a). The elemental ratios of iron and phosphorus to the major elements in the section (calcium, silicon and aluminium) [Fe/(Ca + Si + Al), P/(Ca + Si + Al)] show similar

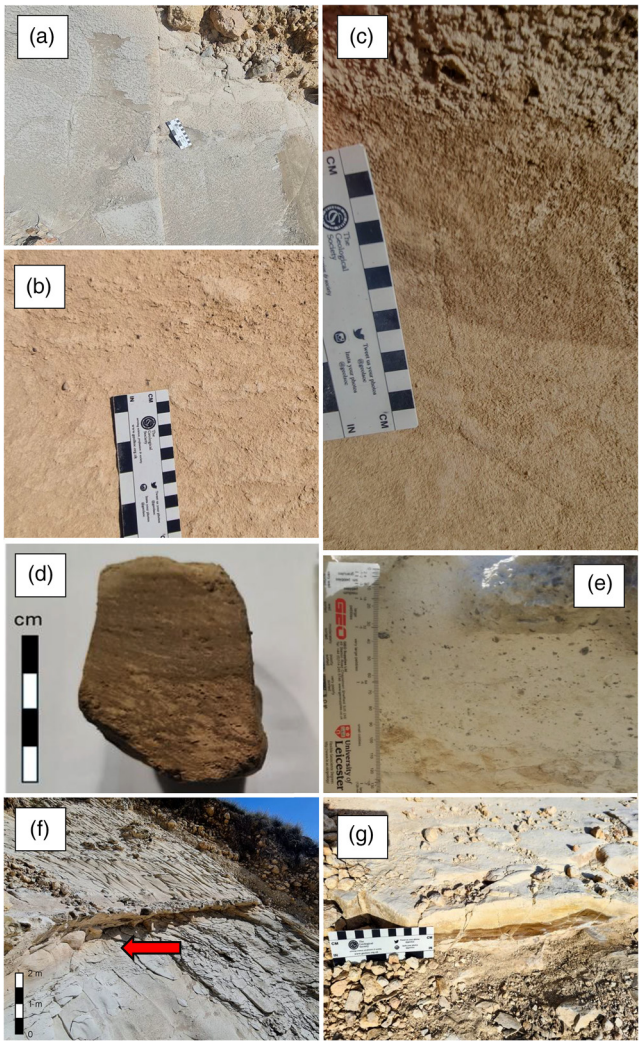

Fig. 3. (**a**) Dark coloured mudstones from SP IV. (**b**) Centimetre-sized allochthonous phosphatic pebbles within the mudstone/wackestone facies of SP V. (**c**) Conformable transition from the SP V mudstone/wackestone associations to the dark mudstones of SP VI. (**d**) The very finely laminated dark green to beige organic-rich mudstones of SP VII. (**e**) Siliceous pebbles at the base of the cherty mudstones of SP VII. (**f**) Arrow indicating continuous sedimentation and the shift from the organic-rich facies of SP VI to the cream-coloured siliceous facies of SP VII. (**g**) Chert nodule (seen in cross-section) occupying space within the muddy siliceous mudstones.

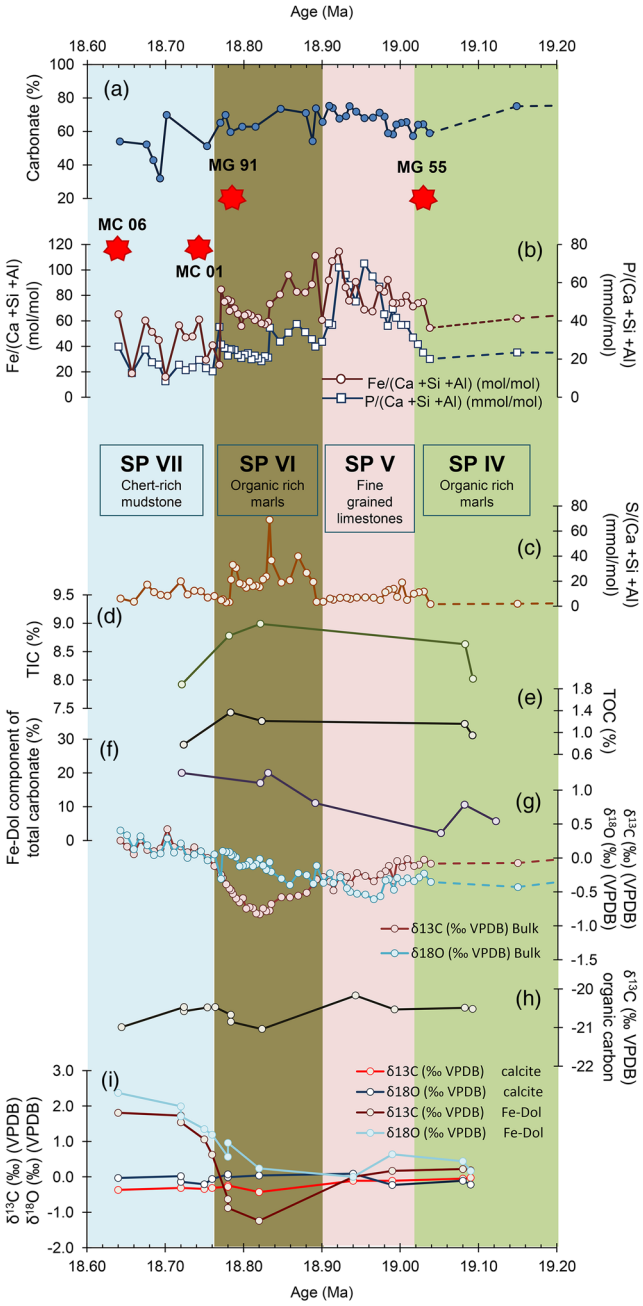

Fig. 4. (**a**) Carbonate content varies throughout the section with notable drop within the cherty SP VII. (**b**) The elemental ratios of Fe and P to major elements (Ca, Si and Al) in the section are generally high within the organic-rich SP VI and drop significantly in SP VII. (**c**) The ratio of S to the major elements follows a similar trend. The total inorganic carbon (TIC) (**d**) shows little variability and the total organic carbon (TOC) (**e**) is generally high for marine carbonates with a maximum value of 1.37% occurring within SP VI. (**f**) The Fe-dolomite component in the total carbonate increases with height in section. (**g**) Bulk stable isotopes ($\delta_{18}O$ and $\delta_{13}C$) show that the $\delta_{13}C$ values shift by ~3 ‰ as the lithology changes from the organic-rich facies of SP VI to the siliceous facies of SP VII and the $\delta_{18}O$ increases by ~2 ‰ for the same lithological change. (**h**) The $\delta_{13}C$ for the organic carbon component varies between −20 and −21‰. The bulk $\delta_{13}C$ (**g**) and the Fe-dolomite $\delta_{13}C$ (**i**) show decreased values associated with the organic-rich SP VI marls, a correlation not observed in the $\delta_{18}O$ records. Both Calcite stable isotope records ($\delta_{18}O$ and $\delta_{13}C$) (**i**) show little variability throughout the section while the Fe-dolomite stable isotopes change significantly. The geochemical records highlight the variability in the stable isotope ($\delta_{18}O$ and $\delta_{13}C$) records of the calcite, Fe-dolomite and C_{org} phases with changes in TOC and percentage components of Ferroan dolomite of the carbonate content.

patterns throughout the studied interval and are generally similar to the ratio of S/(Ca + Si + Al). These ratios are generally high within SP V and SP VI, decreasing significantly within the cherty SP VII (Fig. 4b, c).

The TIC content remains unchanged throughout most of the succession, with values ranging between 8.0 and 9.0% by weight. Peak values of *c.* 9.0% are present within the dark SP VI carbonate mudstones, dipping to *c.* 8.0% in the cherty mudstones of SP VII. The trend remains the same as that of the carbonate content, as expected (Fig. 4d). The TOC content is generally high for marine carbonates throughout the section, with the lowest value of 0.78% occurring within the cherty SP VII. The highest TOC value of 1.37% is found near the top of SP VI (Fig. 4e), corresponding to the darker and most finely laminated parts of the section.

The semi-quantitative EDS analysis revealed that iron carbonate in the cements never exceeds 25% by mass, suggesting a composition more consistent with dolomite or intermediate members of the dolomite–ankerite series (i.e. ferroan dolomite) given that calcium

remains at *c.* 50% of the total cation content (Supplementary Material, Table S3). The contribution of the iron dolomite component of the total carbonate tends to increase with height in the section, reaching a maximum of 20% within the organic-rich SP IV beds and remaining high in the overlying cherty beds of SP VII (Fig. 4f). A similar trend was previously observed in Maltese outcrops at il-Qammieħ and Xatt l-Aħmar, suggesting that this is a regional signal and not local to il-Blata (John *et al.* 2003).

The stable isotopes ($\delta^{18}O$ and $\delta^{13}C$) in the calcite mineral phase of the studied samples tend to remain similar throughout the interval with very little variability (Fig. 4i). However, the same cannot be said about the $\delta^{18}O$ and $\delta^{13}C$ measured in the iron dolomite component of the total carbonate (Fig. 4i). Both $\delta^{18}O$ and $\delta^{13}C$ show considerable variation, with $\delta^{13}C$ reaching a minimum of −1.24‰ within the organic-rich SP VI samples and then increasing significantly to 1.81‰ within the cherty interval of SP VII. The lowest value for $\delta^{18}O$ is 0‰ in SP V and a maximum of 2.37‰ within SP VII. The $\delta^{18}O$ values increase by *c.* 2‰ in the shift from the organic-rich SP VI interval to the silica-rich SP VII interval, whereas the change in $\delta^{13}C$ for the same interval is *c.* 3‰. In general, the lowest values of iron dolomite $\delta^{13}C$ have a good correspondence with the lowest values in the bulk rock $\delta^{13}C$ record and coincide with lowest values of $\delta^{13}C$ in organic carbon and high TOC levels (Fig. 4h).

Petrographic analysis

In general, all the samples display fine crystalline matrix-selective dolomitization. The dolomite crystals are 4–20 μm in size, planar-e to planar-s, and are usually zoned. As shown by the SEM-EDS analyses, the dolomite is iron-rich (4.1–24.9% by weight). The crystals within SP IV (sample MG 55) present zoning that consists of alternations of variably calcium- and iron-rich bands (Fig. 5a). The calcitic foraminiferal tests typically consist of a micrite and/or microspar matrix and are at times punctually phosphatized. Isopachous dogtooth fringes overlain by blocky calcite crystals are often observed in different parts of the section (SP VI and SP VII) (Fig. 5b–d). The silicification of planar-e rhombohedral crystals is commonly observed, but, interestingly, the process does not appear to have affected calcitic foraminiferal tests. Opal lepispheres were observed in SP VII (Fig. 5e). Putative prokaryote cells appear to be preserved in intra-chamber cements (SP IV) and, at times, there are also spar and microspar aggregates presenting textures suggestive of precipitation in microbial exopolymers (Fig. 5f). These include mucilage strings and spheroidal features comprised of nanocrystalline carbonate (Bontognali *et al.* 2008).

Pyrite was observed in all the samples, appearing as framboids with composite diameters ranging from *c.* 3 to *c.* 11 μm and comprised of individual crystallites at the nanometre scale (<400 nm). Pyrite also occurs as the (presumed) replacement of aragonitic pellets, but it is notably absent as single crystals. Framboidal pyrite can either occur in the matrix (SP VII) (Fig. 5g, h) or, as in SP IV, infilling the chambers of planktonic foraminifera (Fig. 5b). Microcrystalline fibrous gypsum can also be found infilling the chambers of foraminifera (MG 91 and MC 06) and this cement is often silicified (Fig. 5i). Gypsum cement was not only observed in the chambers of planktonic foraminifera species, but also in the large elongated benthic foraminifera present in SP VII (Fig. 5j).

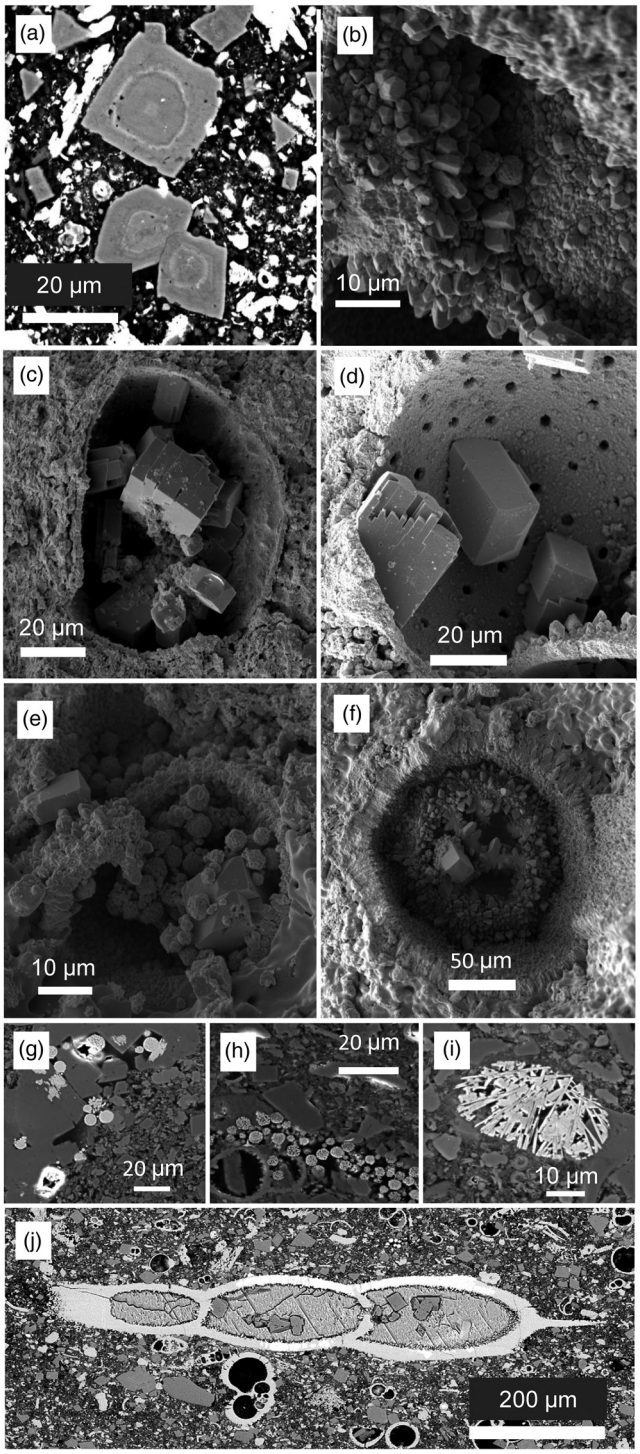

Fig. 5. (**a**) Zoned dolomite crystals displaying calcium-rich and iron-rich bands (MG 55, SP IV). (**b**) Dolomite crystals (MG 55 SP IV). (**c**) Blocky calcite crystals in a foraminiferal test (MG 91, SP VI). (**d**) Inner test of a well-preserved planktonic foraminifera containing blocky calcite crystals (MC 01, SP VII). (**e**) Lepisphere-like forms and calcite crystals inside a recrystallized foraminiferal test (MC 06, SP VII), (**f**) bacterial activity in the form of mucilage strings inside a dolomitized foraminiferal test (MG 55, SP IV). (**g**) Large framboids *c.* 10 μm (MG 91, SP VI). (**h**) Small framboids within a matrix (MC 06, SP VII). (**i**) Microcrystalline fibrous gypsum filling benthic foraminifera (MG 91, SP VI). (**j**) Gypsum and calcite cement inside elongate benthic foraminifera (MC 06, SP VII).

Discussion

Indicators of stratification of the Central Mediterranean water column during an Early Miocene anoxic event

The framboids present within planktic foraminiferal tests and in the muddy matrix were observed via SEM in all representative samples (Fig. 5b, g, h). Framboid sizes can be indicative of the environment of deposition (Rickard 2019). Our data from the il-Blata records demonstrate differences in the mean framboid size between the organic-rich section (SP VI) and the rest of the samples. In general,

the mean framboid sizes are considered to be small and never >10 μm, suggestive of pyrite growth within an anoxic and sulfur-rich water column (Wilkin *et al.* 1996). Pyrite tends to accumulate and grow into larger framboid sizes (from 10 μm up to 40 μm) once the particles settle on the seafloor and grow in fluids supersaturated with iron sulfide (Wilkin *et al.* 1997). Such conditions are best achieved in settings characterized by Eh fluctuations, where polysulfide intermediates can be cycled (Ohfuji and Rickard 2005). The presence of small (<10 μm) framboids in foraminiferal tests suggests that these conditions may have developed in the water column (Rickard 2019).

The framboid sizes within the most organic-rich (TOC *c.* 1.4%), finely laminated SP VI layers tend to be generally larger than the framboids within the rest of the section (Fig. 5g). This general increase in framboid diameter (mean *c.* 7 μm), coupled with the very fine laminations and no clear indication of bioturbation (Fig. 3d) within this sedimentary package, highlights a change in the sedimentary environment. Framboids with diameters of *c.* 6–10 μm can be indicative of weakly oxygenated bottom waters (lower dysoxic), as seen in finely laminated and non-bioturbated sediments (Wignall and Newton 1998). This aligns with the sedimentary characteristics of SP VI at il-Blata. However, the formation of framboidal pyrite can also occur during early burial in the sediment rather than in the water column. The lack of single crystals and the observed replacement textures suggest an excess of reactants (iron and polysulfides) in the system, which supports the potential for pyrite growth within the sediment under evolving redox conditions (Bond and Wignall 2010).

The presence of gypsum in SP VI (Fig. 5i) further highlights this change and – coupled with the high sulfur concentrations, elevated iron and phosphorus to major element ratios and a significant negative spike in bulk $\delta^{13}C$ coinciding with a negative excursion in both iron dolomite and organic carbon $\delta^{13}C$ – indicates early diagenesis under a ferruginous (high iron, low sulfide) setting that precludes significant sulfate reduction (Fig. 5b, c, g and i). This also coincides with the layer containing a high proportion of iron dolomite (Fig. 5f). These reactions would occur very close to the seafloor within centuries or millennia in a way similar to that previously documented in the Eastern Mediterranean.

In the organic-rich, deep-water Late Miocene (Messinian)–Pleistocene sediments of the Eastern Mediterranean, sulfate reduction and the formation of authigenic minerals occur within decimetres below the seafloor, as documented at the Integrated Ocean Drilling Program and Deep Sea Drilling Project Leg 42A Sites 374 (Messina Abyssal Plain) and 376 (Florence Rise) (Sigl *et al.* 1978). Cores from these sites reveal sulfur–iron interactions, such as dolomite cementation features, at times accompanied by gypsum (Passier and De Lange 1998). Importantly, for these processes to occur, the effects of organic matter reduction must be paired with a source of alkalinity to counteract changes in pH during precipitation (Rubin-Blum *et al.* 2014; Sela-Adler *et al.* 2015; Petrash *et al.* 2017; Wurgaft *et al.* 2019; Sisma-Ventura *et al.* 2022). This alkalinity might be sourced from riverine base cation and soil-derived nutrient inputs, or from the dissolution of carbonate in the sediment. We discuss the additional influence of riverine inputs on the sedimentary deposits at il-Blata in the following text.

The excess Fe^{2+} incorporated into dolomite and, to a minor extent, framboidal pyrite could be supplied by two main sources: (1) atmospheric deposition and (2) fluvial fluxes. However, in an oligotrophic configuration, exclusive fertilization by dust would not be sufficient (Herut *et al.* 2002) and upwelling systems are, for the most part, iron-limited (Frost and Franzen 1992; Hutchins *et al.* 2002). A fluvial input therefore has to be considered to achieve the excess nutrients conducive to oxygen depletion and to have an excess of iron in the environment. In this scenario, the presence of iron dolomite and the preservation of carbonates in the il-Blata section supports models of enhanced continental runoff into the Central Mediterranean during the Early Miocene, in a similar way to that observed in the Miocene Monterey Formation (Baker and Burns 1985). The terrigenous fluxes deliver ferric (Fe^{3+}) iron, while decomposing organic matter produces the reducing conditions necessary for the solubilization of reducible iron in the pore waters, followed by its incorporation into dolomite. These terrigenous inputs also alter the pore water biogeochemistry, increasing microbial activity and promoting pore water dolomite saturation via the generation of alkalinity.

Alternative dolomitization models do not appear to be applicable here. The burial depth, local thermal gradient and lack of evidence for thermogenic fluid migration precludes thermogenic dolomitization. Additionally, the palaeogeography and depositional water depth do not support the conditions necessary for mixing zone dolomitization (Dart *et al.* 1993; Bellanca *et al.* 2002). Although the presence of gypsum might, under a coastal depositional scenario, suggest a reflux dolomitization path, the absence of any known lagoonal facies in the Pelagian Islands during this period challenges this model (Pedley *et al.* 1978; Pedley 1996). Therefore, in the depositional context of the Globigerina Limestone Formation, gypsum is more likely to be a by-product of sedimentary sulfur cycling occurring beneath a density- and redox-stratified water column (Petrash *et al.* 2022). In line with our fluvial input interpretation, dolomite can be attributed to a stage of increased bottom currents that caused submarine erosion and facilitated the inflow of ferric iron-bearing particles into the anoxic bottom waters overlying organic-rich seafloor sediments. The presence of iron dolomite and, to a lesser extent, pyrite, strongly indicates significant iron reduction and redox gradients, emphasizing the importance of early diagenetic iron reduction in organic-rich sediments. Burial diagenesis further enhanced the utility of any early formed dolomite precursors as valuable proxies for reconstructing the palaeoenvironmental conditions (Bathurst 1987; Bottrell and Raiswell 1989), leading to the strata-bound abundance of dolomite that we observe in the il-Blata section.

The decoupling between the bulk stable isotope records for $\delta^{18}O$ and $\delta^{13}C$ within SP VI (18.90–18.76 Ma) and the deviation of these values from global benthic records (Figs 4g, 6a) can now be discussed. The reason for this decoupling can be attributed to a changing depositional environment and its effects on early diagenesis, the establishment of redox zonation within the water column and the mineral-specific stable isotope composition (Blanchet *et al.* 2021). The iron dolomite at the il-Blata section exhibits $\delta^{13}C$ values (Fig. 4i) that are less negative than those of dissolved inorganic carbon (DIC) from iron-reducing environments (Curtis *et al.* 1986), which suggests a mixed carbonate ion source. This isotopic signature likely results from the partial contribution of DIC from Early Miocene seawater and ^{13}C-depleted carbon from organic matter oxidation under iron-reducing conditions. The substitution of Mg^{2+} (and Ca^{2+}) by Fe^{2+} in dolomite lattices indicates ferruginous, anoxic pore waters, where Fe^{2+} ions can accumulate and be incorporated into the dolomite lattice (Barnaby and Rimstidt 1989; Clarkson *et al.* 2014). Iron is incorporated into the carbonate crystal lattice when it occurs in the ferrous (Fe^{2+}) ionic state and this is controlled by reducing pore waters. Pore waters poor in oxygen can facilitate the accumulation of Fe^{2+} ions, which can be incorporated into diagenetic carbonates. The conditions facilitating Fe^{2+} and Mg^{2+} co-precipitation with Ca^{2+} into dolomite were likely driven by chemolithotrophic respiration sustaining alkalinity production and proton consumption in the pore waters during growth (Petrash *et al.* 2017, 2021).

Notably, the peak formation of iron dolomite in SP VI is associated with a negative $\delta^{13}C$ excursion in the bulk record (Fig. 4f, g), indicating that these stratigraphic levels likely formed during the peak of ferric iron reduction and during shallow burial. This likely

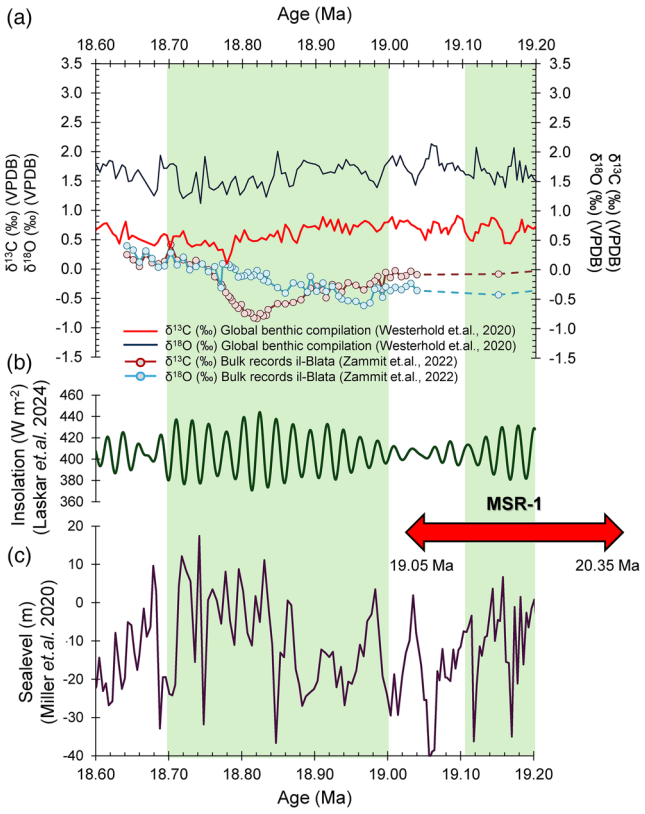

Fig. 6. (**a**) Global benthic and bulk il-Blata carbonate stable isotope records. The bulk il-Blata $\delta^{13}C$ records demonstrate a notable negative shift in the organic-rich facies of SP VI. This is concomitant with a peak in the insolation variability (*c.* 400 kyr cycle) (**b**) and occurred around a trough in global sea-levels (**c**). Rising sea-levels may be associated with a positive shift in stable isotope records and the emplacement of siliceous deposits. The MSR-1 seaway restriction occurred between 20.35 and 19.05 Ma, coinciding with a trough in global sea-level (Zammit *et al.* 2022).

occurred in the absence of substantial concentrations of sulfide as a by-product of microbial sulfate reduction, which would have otherwise titrated iron out from the pore waters as pyrite and prevented the substantial co-precipitation with magnesium and calcium in carbonate phases observed across the studied section (Berner 1984; Raiswell and Canfield 1998; Poulton and Canfield 2005). However, in the absence of iron, organic matter can absorb the excess sulfur through a 'vulcanization' process, rendering it inaccessible for microbial respiration (Sinninghe Damst'e *et al.* 1989; Aizenshtat *et al.* 1995; Urban *et al.* 1999).

A subsequent shift towards positive $\delta^{13}C$ values in the iron dolomite component is observed in the upper sedimentary packages (Fig. 4g). This points to a shift in the fluid-buffered diagenetic environment where iron dolomite formed. Open diagenetic systems are fluid-buffered in the shallow to intermediate burial realm, with isotope exchange dominated by pore fluid flow through partially lithified carbonate sediments (fluid-controlled) (Bjørlykke and Jahren 2012; Higgins *et al.* 2018). Such a shift possibly coincided with changing basin redox stratification conditions, or was the result of the changing contribution of seawater v. formation waters in the precipitation milieu, previously conditioned to high carbonate precipitation rates (Immenhauser 2022). Additionally, the presence of significant chert in these layers, coupled with a decrease in iron to major element ratios (Fig. 4b) in the bulk sediment record, is also indicative of changes in the oxidation and mineral saturation state of the sediments (Clarkson *et al.* 2014).

Changes in nannofossil assemblages can also be an indicator of enhanced land surface runoff leading to the establishment of eutrophic surface waters (Auer *et al.* 2014). In this regard, the increased presence of *Helicosphaera carteri* in the studied section (Baldassini and Di Stefano 2015) may be indicative of eutrophic surface conditions and a strong input of terrigenous material (Auer *et al.* 2014; Oretade 2021). However, other taxons indicative of these conditions have not been reported and, coupled with the fact that this taxon remains high throughout the section, this may preclude its validity as a useful indicator. This argument in itself does not present the fully quantitative and systematic palaeoecological study that is needed to properly make these claims. In the absence of such, the available data offer only limited constraints on the trophic conditions in the region.

Significant amounts of silica in the upper layers (SP VII), coupled with a decrease in the iron to major elements ratio in the bulk record, are suggestive of a change in the oxidation and saturation state of the basin recorded in the sediments (Fig. 4b). The clay-rich nature of the underlying SP VI layer may have prevented the silicification of the underlying sediments by offering a barrier to the overlying fluids. The silica is concentrated in the chert nodules seen in specific horizontal layers in an almost periodic pattern. This may suggest that the processes leading to their formation were associated with cyclical blooms of siliceous organisms in surface waters impacted by iron 'fertilization' (Li *et al.* 2022). The oxidation of organic matter within carbonate-rich sediments is considered to be a possible mechanism for nodular chert formation at sites where 'carbonate ghosts' are replaced by chert nodules (Fig. 3g) (Maliva and Siever 1989).

In addition, a shallow burial silicification mechanism for carbonate may be driven by alkaline (i.e. silica-oversaturated) fluids permeating the bottom of the stratified column and diffusing into the upper sediments, where the fluid input could lead to the partial replacement of early formed dolomite cements (Petrash *et al.* 2016 and references cited therein). This silica-rich fluid could have induced the development of a coupled dissolution–precipitation reaction front, leading to the pseudomorphic replacement of metastable calcium-rich precursors to dolomite. However, the already stabilized (to calcite) micritic fabrics of foraminifera, as well as the more stable pre-existing early diagenetic/primary (magnesium-rich) dolomite (see Meister *et al.* 2022), were not silicified. The replacement of metastable early diagenetic carbonates by silica is believed to occur under shallow burial diagenetic conditions under the influence of diagenetically evolved seawater. The pore waters would have possibly been saturated with regard to gypsum, as evidenced by the presence of pseudomorphic gypsum partially silicified within benthic foraminifera chambers (Fig. 5i, j). Density stratification in isolated basin settings is conducive to the diagenetic processes evaluated here and is also responsible for the establishment of bottom water anoxia (Meyer and Kump 2008).

The TOC measured in this study (Fig. 4e) is generally high for marine carbonates and is highest in the dark green, finely laminated mudstones pertaining to SP VI, with a maximum value of 1.37%. The definition originally proposed by Kidd *et al.* (1978) considers pelagic mudrocks containing between 0.5 and 2% by weight to be 'sapropelic' and distinct pelagic layers thicker than 1 cm containing >2% TOC to be true 'sapropels'. Using this definition, the layers investigated here are defined as 'sapropelic'. Their dark and finely laminated nature also define them as such (Cramp and O'Sullivan 1999). This makes the il-Blata organic-rich layers very important sapropelic deposits from relatively shallow pelagic environments at a time when no such deposit was widespread in the Mediterranean. This further highlights the importance of land-based sections in our understanding of climatic evolution and justifies the search for further land or deep sea sections that can offer insights into the evolution of the climate during the Early Miocene. In particular, the regional and global climate dynamics during the Burdigalian are poorly known. The initial closure of the Mesopotamian Seaway

(Bialik *et al.* 2019) at this time, the end of low-latitude phosphatization (Föllmi *et al.* 2008; Zammit *et al.* 2022) and a global shark extinction event suggest that this time period merits further investigation (Sibert and Rubin 2021).

It is encouraging to note similarities in lithostratigraphy and minerology with other sites outcropping in the Maltese Islands (John *et al.* 2003), Sicily (Föllmi *et al.* 2008), Central Italy (Cornacchia *et al.* 2022; Auer *et al.* 2015, 2016; Brandano *et al.* 2016) and North Africa (Riahi *et al.* 2015; Essid *et al.* 2019); however, due to numerous hiatuses and, at times, the limited age constraints of the sections, a precise stratigraphic correlation between these sites remains problematic. This makes the il-Blata section an important site in understanding the evolution of the Mediterranean basin and its unique tectono-climate characteristics and also highlights the need for further detailed investigation of the il-Blata site and stratigraphic correlation between il-Blata and other contemporaneous outcrops in the region.

Climatically controlled Central Mediterranean sedimentary processes

The Maltese depositional environment underwent a dramatic change following MSR-1 (20.35–19.05 Ma), with a shift from low sedimentation rate phosphorite-bearing marine limestones to high sedimentation rate continentally influenced mudstones (Zammit *et al.* 2022). A decrease in the carbonate content observed within the studied interval can be correlated with the influx of continental material via riverine systems that were activated at this time and flooded the low-productivity marine system. Our new records allow us to further understand the climatic history of the Central Mediterranean in finer detail. As previously proposed (Bialik *et al.* 2019; Zammit *et al.* 2022), the tectonic and eustatically forced decrease in surface water flow through the Mesopotamian Seaway had a direct effect on the North African hydroclimate by favouring the intensification of the Atlantic circulation.

As the newly enclosed Mediterranean basin became more sensitive to the modified circulation effects, the seasonality of monsoonal activity, which is strongly modified by eccentricity (Wu *et al.* 2021), enhanced the delivery of terrigenous material sourced from North Africa. This created palaeoproductivity plumes in the surface Mediterranean waters that had a transient excess of bio-limiting nutrients, such as iron and silica. An estimate of the extension and areal sensibility of these Early Miocene plumes to minor changes in flux can be provided by considering the extension of Nile plumes prior to the construction of the Aswan High Dam in Egypt. Before the construction of the dam, the Nile plume extended as far north as Beirut during peak activity (Oren 1969). Considering that Beirut is >400 km from the edge of the Nile Delta, it is reasonable to assume a similar range as the minimum extension. It is also likely that the extent of these plumes was larger during the peak fluxes associated with sapropelic events. It can therefore be assumed that any active fluvial system in Libya and Tunisia (e.g. the Fezzan and Chott systems; Fig. 1) may have had plumes extending well into the area of the Maltese Islands during peak activity (Fig. 7a). In a Mediterranean flow system conditioned by a closed eastern gateway, surface waters entering from the Atlantic Ocean would have moved eastward and carried the Chott plume from the Gulf of Gabes into the Central Mediterranean (Fig. 7a). This would make the Chott system a more likely source of inorganic material over Malta than the Fezzan system that outflows from the Gulf of Sirte because the surface flow would have carried a plume from Sirte away from Malta.

Within the context of orbital forcing, high seasonality would result from times when the Earth's tilt, precession and eccentricity produced significant seasonal contrasts. The difference between summer and winter temperatures is heightened during these periods.

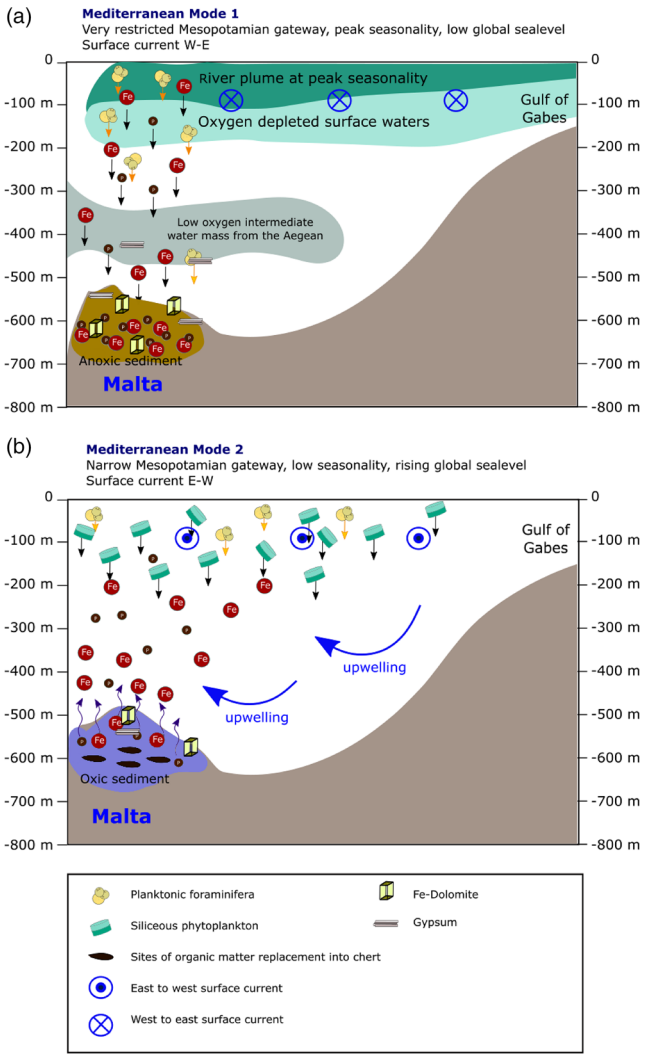

Fig. 7. (**a**) With a heavily restricted Mesopotamian gateway, surface waters flow towards the east and help carry river plumes from the Gulf of Gabes over Malta. The closed gateway also favours intense hydroclimatic activity over the western Sahara, with a large plume extending into the Central Mediterranean during peak insolation variability. In combination with low-oxygen intermediate waters coming from the Aegean, this generates anoxic conditions in the region. (**b**) A re-opened Mesopotamian gateway helps to restore vertical mixing, reoxygenating the sediments and releasing iron and phosphorus into the water column. This also activates upwelling and results in a siliceous phytoplankton bloom. Silica is lithified in sites with oxidized organic matter, resulting in the formation of nodular cherts.

This increased seasonality causes the surface waters to warm significantly in summer, creating a strong thermocline – that is, a steep temperature gradient between the warm surface waters and the cooler, deeper waters. This thermocline acts as a barrier to vertical mixing, leading to a highly stratified water column (Grant *et al.* 2016). As a result, the deep waters can become anoxic because the oxygen consumed by biological processes is not replenished by mixing with the oxygen-rich surface waters. We propose that an enhanced supply of terrigenous material from the Gulf of Gabes drove up productivity and led to the establishment of poor oxygen conditions in the water column. The introduction of low-oxygen intermediate waters from the Aegean region is also possible in this closed eastern gateway configuration (Zirks *et al.* 2019) (Fig. 7a). This flux of oxygen-poor intermediate waters from the Aegean could also have facilitated the formation of oxygen minimum zones.

Within the limitations of our data, it is possible to present a hypothesis that the peak of iron dolomite generation, peak TOC and

negative $\delta^{13}C$ excursion coincided with a time of maximum eccentricity (400 kyr cycle) and the greatest peak-to-peak fluctuations in the precession cycle (Fig. 6). However, because the site has not yet been astronomically tuned, this hypothesis needs to be evaluated with caution and the following inferences are only suggestions. The formation of iron dolomite can be attributed to early diagenesis influenced by a combination of an enclosed Mediterranean Sea, generating the necessary ocean current systems, and the right conditions for intermediate low-oxygen waters forming in the Aegean region, astronomically modulated by a *c.* 400 kyr cycle. It would be instructive to resample the il-Blata section at very high resolution and to test this hypothesis to confirm or deny the influence of astronomical forcing factors on the depositional and diagenetic trends observed. The fact that anoxic sediments in the Mediterranean can be modulated by a *c.* 400 kyr cycle has previously been reported for Mid-Miocene phosphorite-bearing carbonate deposition in Central Italy (Auer *et al.* 2016).

Redox-controlled siliceous productivity bloom

Iron-bound phosphorus can be incorporated as phosphates in sediments featuring euxinic (i.e. high sulfide anoxic) conditions (Dijkstra *et al.* 2014). The data presented here indicate an association between iron and phosphorus, although such data need to be considered with caution because X-ray fluorescence records are semi-quantitative and no extraction procedure was used in the determination of phosphorus. Still, there is a general correspondence between the iron and phosphorus records. The amounts of phosphorus and iron trapped in the sediments changes swiftly with the lithological change to cherty limestones and the rapid shift in the iron dolomite stable isotope records (Fig. 4b, i). Both iron and phosphorus can be re-released into pore waters when the oxygenation state changes (Filippelli *et al.* 2003).

It is likely that, following the peak in hydrological activity over North Africa at 18.82 Ma, the decrease in the nutrient flux into the Central Mediterranean and the possibly eustatically mediated (Miller *et al.* 2020) re-opening of the Mesopotamian gateway allowed the return of a mixed and oxygenated water column (Figs 6c, 7b). Such a system would have favoured the remobilization of iron and phosphorus back into the water column, while upwelling systems could have aided the return of these bio-limiting nutrients to the surface. A silica phytoplankton bloom would have ensued, which can account for the increased silica saturation in the sediments.

Evidence for a bloom in siliceous organisms can also be attained by noting a peak in the abundance of the zeolite mineral clinoptilolite recorded in the Middle Globigerina Limestone Member (John *et al.* 2003). Although John *et al.* (2003) attribute this peak in clinoptilolite to a volcanic input, the presence of siliceous deposits at il-Blata and the lack of evidence for regional volcanism during the Early Miocene more likely suggest that the zeolite is indicative of a siliceous bioproductivity bloom (Karpoff *et al.* 2007). This is further supported by records from North Africa showing that the siliceous deposits associated with the Early Miocene Numidian Formation are of biogenic and not volcanic origin (Ben Yahia *et al.* 2019; Essid *et al.* 2019). As biogenic silica fell to the seafloor, the newly available oxygenated state would have decomposed organic matter in the carbonate matrix, creating the conditions for silicification in spaces vacated by the 'ghosts' of carbonate precursors (Figs 3g, 7b) (Maliva and Siever 1989).

The change from a foraminifera-dominated to a siliceous plankton-dominated surface environment might be attributed to a number of factors. Possible general global warming conditions at the time (Westerhold *et al.* 2020), coupled with a high DIC content, may have inhibited planktonic foraminifera, as evidenced by the poor preservation and generally small-sized planktonic forms. The availability of silica from continental sources, coupled with the release of iron and phosphorus from the sediments, could have led to a short-lived (18.76–18.62 Ma) bloom in siliceous organisms during a time of low seasonality. The Central Mediterranean shifted again to a foraminifera-dominated (Mourik *et al.* 2011), phosphorite-bearing (Föllmi *et al.* 2008) marine system following this episode, in conjunction with the global shift in climate associated with the Monterey excursion (Jacobs *et al.* 1996). The global Monterey excursion would have led to high sea-levels, triggering the intermittent re-opening of the Mesopotamian Seaway and influencing upwelling systems in the region until the permanent closure of the Mesopotamian Seaway (MSR-2) during the Mid-Miocene expansion of the Antarctic ice sheet (*c.* 14 Ma).

Early Miocene organic-rich facies in the Central Mediterranean: the oldest Mediterranean sapropelic deposits?

The present day circulation in the Mediterranean Sea is driven by density changes, whereby warm, fresh Atlantic surface waters (salinity *c.* 36 PSI, temperature *c.* 16°C) (Béranger *et al.* 2005) entering from the Strait of Gibraltar are transformed into salty, cool intermediate waters via intense evaporation in the (mostly) northern parts of the Eastern Basin (Brenner 2012). This intense halothermal circulation and the enclosed nature of the basin is conducive to the formation of well-oxidized surface waters reaching the seafloor, resulting in a well-oxygenated water column (Rohling *et al.* 2015). However, this configuration was not a constant feature of the region throughout its geological history.

Periodic episodes of oxygen starvation in Mediterranean bottom waters have been recorded in the Mediterranean basin since the Early to Mid-Miocene (Taylforth *et al.* 2014; Rohling *et al.* 2015; Athanasiou *et al.* 2021; Bialik *et al.* 2022). These are associated with periods of high seasonality in orbital parameters (maximum eccentricity) (Mancini *et al.* 2023). Evidence of these episodes comes from the deposition of sapropels, which can serve as an indication of shifts in the general mode of circulation.

During the Pleistocene, these perturbations in the general circulation and stratification of the water column were driven by surges in freshwater inputs, such as those from the Nile during times associated with high northern summer insolation (Grant *et al.* 2016). It has generally been considered that the input of low-density fresh water can generate a highly stratified water column, which, coupled with high fluxes of DIC in surface waters, can lead to the high utilization of oxygen in surface layers. This, in turn, results in the eventual depletion of oxygen further down the water column and the formation of oxygen minimum zones (Blanchet *et al.* 2021).

It has been suggested that a key component in the formation of sapropels in the Eastern Mediterranean is the formation of an intermediate water mass depleted in oxygen, but which is neither anoxic nor euxinic (Zirks *et al.* 2019). It has been shown that, during the Holocene (*c.* 8.2 ka), such a water mass formed in the Aegean and migrated both east and west, reaching the Levantine basin in the SE and the Adriatic basin towards the west. The oxygen dissolved in this water mass progressively decreased as these intermediate waters moved towards the Nile delta plume and encountered sinking dissolved inorganic matter (Zirks *et al.* 2019). Sapropel formation in the Mediterranean can therefore be seen as being driven by the formation of an intermediate water mass poor in oxygen in combination with a strong seasonal component affecting the discharge of the Nile. Such an intermediate water mass would be formed due to climatic reasons associated with global cooling driving enhanced convection in the enclosed Aegean region (Filippidi *et al.* 2016; Filippidi and De Lange 2019).

The transition to an enclosed configuration in the Miocene would have favoured the formation of these organic-rich layers. Geological

evidence for the existence of early Mediterranean sapropels supports this interpretation. Unambiguous sapropelic layers first appear (13.5 Ma) following the final closure of the Eastern Mediterranean Seaway (MSR-2 at *c.* 14 Ma) (Grant *et al.* 2016) and it seems reasonable to assume that only an enclosed basin favours a circulation pattern conducive to periodic bottom water anoxia. There is also evidence for older 'proto-sapropelic' organic-rich layers from field outcrops in Cyprus dated to *c.* 15.5 Ma (Athanasiou *et al.* 2021; Bialik *et al.* 2022). It is now known that the eastern gateway had already been severely restricted during the Early Miocene (MSR-1) (Bialik *et al.* 2019; Zammit *et al.* 2022), raising the possibility of water column stagnation during times of low east to west oceanic surface water flows. There is also the possibility that this gateway was intermittently re-opened during the Miocene climatic optimum at *c.* 17 Ma (Cornacchia *et al.* 2021) via eustatic control and that an enclosed basin configuration existed for a geologically short-lived interval between MSR-1 (*c.* 20 Ma) and the Miocene climatic optimum (*c.* 17 Ma).

It has been proposed that the shift from predominantly marine limestones bearing phosphatic hardgrounds to clay-/mud-rich facies pertaining to the Middle Globigerina Limestone Formation in Malta was the result of a shifting climate over western North Africa (Zammit *et al.* 2022). This shift towards a wetter climate has been considered to be a land–atmosphere–ocean response to gateway changes causing an intensification of the Atlantic circulation and the ensuing climatic influence on the North African land mass (Zammit *et al.* 2022). Depositional Interval 2 of the il-Blata facies investigated in this study was deposited during this short period in which Mediterranean surface water flow from the east was severely reduced and the long-standing east–west surface flow was switched to a west–east flow, sinking in the east in a thermohaline conveyor system. Coupling the increased runoff from North Africa with the new circulation system and the possibility of the formation of de-oxygenated intermediate waters (in the northern basins of the Eastern Mediterranean), it is very likely that anoxic (ferruginous) and/or transiently euxinic conditions formed in the pelagic/hemipelagic zones of the Central Mediterranean and influenced the subsurface stabilization of iron dolomite in the sediments of the il-Blata section.

The presence of planktonic foraminifera infilled by gypsum may indicate that density saturation was established in the water column at the time of deposition These gypsum-saturated waters may also have been established at the sediment–water interface, leading to pore water oversaturation with respect to gypsum, with the mineral accumulating in the chambers of benthic foraminifera. These density- and redox-stratified conditions favoured the accumulation of organic matter, with the TOC content measured in this study generally being high for marine carbonates. A maximum value of 1.37% in SP VI indicates that sapropelic layers formed within this sedimentary package. The possible re-opening of the Mesopotamian Seaway precluded the low-oxygen conditions and increased ventilation throughout the water column. A combination of available oxygen and nutrients led to a short-lived siliceous plankton bloom, as evidenced in the chert nodules of SP VII. Further examination of the gypsum infilling discrete foraminiferal chambers using stable $\delta^{18}O$ and $\delta^{34}S$ isotopes would provide further insights, but this would require high-resolution *in situ* analyses, such as NanoSIMS.

Conclusions

The formation of iron dolomite, sapropelic layers and chert in the outcrops of the Middle Globigerina Limestone Member in Malta was the result of a combination of interrelated factors. Foremost among these was the proximity of the Maltese Islands to now-extinct North African fluvial systems, particularly on the western side of the continent. These systems delivered fresh water, nutrients and iron to the surface waters, promoting a stratified water column and oxygen-depleted bottom waters featuring transient ferruginous states. The deltaic systems of the Gulf of Gabes likely had a significant role as the primary sources of iron into the marine realm, facilitating the formation of iron dolomite at sites such as il-Blata in Malta.

During the peak activity of these fluvial systems, the surface waters in the Central Mediterranean became highly stratified with limited oxygen availability. Organic matter decomposition under these conditions generated alkalinity and the establishment of reducing environments below the sediment–water interface, facilitating the solubilization of ferrous iron into pore waters oversaturated with respect to carbonate. This ferrous iron, along with magnesium and calcium, was incorporated into early nucleated dolomite lattices under conditions of subsurface chemolithotrophic respiration, which promoted carbonate growth. The peak of these conditions, at *c.* 18.82 Ma, coincided with preserved sapropelic layers, marked by an elevated TOC content and negative $\delta^{13}C$ excursions. These layers highlight ferric iron reduction processes, where the availability of iron exceeded that of the by-product sulfide, precluding the formation of extensive pyrite and instead favouring iron dolomite precipitation. Burial diagenesis further enhanced these dolomite precursors, stabilizing them as palaeo-environmental proxies for reconstructing the redox and depositional conditions in the Early Miocene.

Subsequent changes in global sea-level re-opened the Mesopotamian Seaway, altering the water dynamics in the Mediterranean. This, combined with climatic changes, re-oxygenated the water column, suppressing the conditions favourable for iron dolomite formation. Instead, re-oxygenation facilitated siliceous productivity blooms, with the oxidation of organic matter and the deposition of silica leading to the formation of chert nodules. These nodules, preserved in SP VII, provide further evidence of the dynamic interplay of diagenetic and depositional processes during this interval. This study underscores the importance of the Mediterranean basin as a natural laboratory for investigating the interconnection between climatic and tectonic controls on sedimentary and diagenetic systems. The detailed records from Malta provide valuable insights into Early Miocene environmental dynamics and diagenetic pathways, particularly the role of fluvial inputs, redox stratification and microbial processes in dolomite formation.

Scientific editing by Neil Davies

Acknowledgements Acknowledgements are due to the Superintendence for Cultural Heritage Malta for permission to collect samples from the il-Blata section (permit SCH213/16). Paul Pearson is thanked for useful discussions. We are extremely grateful to Cedric John for constructive criticism and to the anonymous reviewer for useful feedback, which has greatly improved this paper from its original form. This is Cardiff EARTH CRediT Contribution 35.

Author contributions **RZ**: conceptualization (equal), data curation (lead), investigation (equal), project administration (lead), validation (equal), visualization (equal), writing – original draft (lead), writing – review and editing (lead); **DAP**: conceptualization (equal), data curation (lead), formal analysis (lead), funding acquisition (equal), investigation (equal), methodology (lead), project administration (equal), writing – review and editing (equal); **OMB**: conceptualization (equal), funding acquisition (equal), investigation (equal), project administration (equal), supervision (equal), writing – review and editing (equal).

Funding Daniel Petrash acknowledges the support of an internal project under the Research Organization Long-term Development Concept of the Czech Geological Survey for the Period 2023–2027. Or. M. Bialik is partially supported by the German (GEOMAR)–Israeli (University of Haifa) Helmholtz International Laboratory 'Eastern Mediterranean Sea as a model for Future Ocean Research' (EMS-FORE).

Competing interests The authors declare that they have no known competing financial interests or personal relationships that could have appeared to influence the work reported in this paper.

Data availability All data generated or analysed during this study are included in this published article (and if present, its supplementary information files).

References

Aizenshtat, Z., Krein, E.B., Vairavamurthy, M.A. and Goldstein, T.P. 1995. Role of sulfur in the transformations of sedimentary organic matter: a mechanistic overview. *American Chemical Society Symposium Series*, **612**, 16–37, https://doi.org/10.1021/BK-1995-0612.CH002

Anastasakis, G.C. and Stanley, D.J. 1984. Sapropels and organic-rich variants in the Mediterranean: sequence development and classification. *Geological Society, London, Special Publications*, **15**, 497–510, https://doi.org/10.1144/GSL.SP.1984.015.01.32

Athanasiou, M., Triantaphyllou, M.V. *et al.* 2021. Reconstruction of oceanographic and environmental conditions in the eastern Mediterranean (Kottafi Hill section, Cyprus Island) during the middle Miocene climate transition. *Revue de Micropaléontologie*, **70**, 100480, https://doi.org/10.1016/J.REVMIC.2020.100480

Auer, G., Piller, W.E. and Harzhauser, M. 2014. High-resolution calcareous nannoplankton palaeoecology as a proxy for small-scale environmental changes in the Early Miocene. *Marine Micropaleontology*, **111**, 53–65, https://doi.org/10.1016/J.MARMICRO.2014.06.005

Auer, G., Piller, W.E., Reuter, M. and Harzhauser, M. 2015. Correlating carbon and oxygen isotope events in early to middle Miocene shallow marine carbonates in the Mediterranean region using orbitally tuned chemostratigraphy and lithostratigraphy. *Paleoceanography and Paleoclimatology*, **30**, 332–352, https://doi.org/10.1002/2014PA002716

Auer, G., Hauzenberger, C.A., Reuter, M. and Piller, W.E. 2016. Orbitally paced phosphogenesis in Mediterranean shallow marine carbonates during the middle Miocene Monterey event. *Geochemistry, Geophysics, Geosystems*, **17**, 1492–1510, https://doi.org/10.1002/2016GC006299

Baker, P.A. and Burns, S.J. 1985. Occurrence and formation of dolomite in organic-rich continental margin sediments. *AAPG Bulletin*, **69**, 1917–1930, https://doi.org/10.1306/94885570-1704-11D7-8645000102C1865D

Baldassini, N. and Di Stefano, A. 2015. New insights on the Oligo-Miocene succession bearing phosphatic layers of the Maltese archipelago. *Italian Journal of Geoscience*, **134**, 355–366, https://doi.org/10.3301/IJG.2014.52

Barnaby, R.J. and Rimstidt, J.D. 1989. Redox conditions of calcite cementation interpreted from Mn and Fe contents of authigenic calcites. *GSA Bulletin*, **101**, 795–804, https://doi.org/10.1130/0016-7606(1989)101<0795:RCOCCI>2.3.CO;2

Barron, E.J. and Peterson, W.H. 1989. Model simulation of the Cretaceous ocean circulation. *Science*, **244**, 684–686, https://doi.org/10.1126/science.244.4905.684

Bathurst, R.G.C. 1987. Diagenetically enhanced bedding in argillaceous platform limestones: stratified cementation and selective compaction. *Sedimentology*, **34**, 749–778, https://doi.org/10.1111/J.1365-3091.1987.TB00801.X

Bellanca, A., Sgarrella, F., Neri, R., Russo, B., Sprovieri, M., Bonaduce, G. and Rocca, D. 2002. Evolution of the Mediterranean basin during the Late Langhian–Early Serravallian: an integrated paleoceanographic approach. *Rivista Italiana di Paleontologia e Stratigrafia*, **108**, 223–239, https://doi.org/10.13130/2039-4942/5472

Ben Yahia, N., Sebei, A., Harris, C., Boussen, S. and Chaabani, F. 2019. Mineralogical and geochemical criteria to identify the origin and the depositional environment of the upper Numidian babouchite siliceous rocks, northwestern Tunisia. *Journal of African Earth Sciences*, **149**, 487–502, https://doi.org/10.1016/j.jafrearsci.2018.09.010

Béranger, K., Mortier, L. and Crépon, M. 2005. Seasonal variability of water transport through the Straits of Gibraltar, Sicily and Corsica, derived from a high-resolution model of the Mediterranean circulation. *Progress in Oceanography*, **66**, 341–364, https://doi.org/10.1016/j.pocean.2004.07.013

Berner, R.A. 1984. Sedimentary pyrite formation: an update. *Geochimica et Cosmochimica Acta*, **48**, 605–615, https://doi.org/10.1016/0016-7037(84)90089-9

Bialik, O.M., Frank, M., Betzler, C., Zammit, R. and Waldmann, N.D. 2019. Two-step closure of the Miocene Indian Ocean Gateway to the Mediterranean. *Scientific Reports*, **9**, 8842, https://doi.org/10.1038/s41598-019-45308-7

Bialik, O.M., Reolid, J., Kulhanek, D.K., Hincke, C., Waldmann, N.D. and Betzler, C. 2022. Sedimentary response to current and nutrient regime rearrangement in the Eastern Mediterranean during the early to middle Miocene (southwestern Cyprus). *Palaeogeography, Palaeoclimatology, Palaeoecology*, **588**, 110819, https://doi.org/10.1016/J.PALAEO.2021.110819

Bjørlykke, K. and Jahren, J. 2012. Open or closed geochemical systems during diagenesis in sedimentary basins: constraints on mass transfer during diagenesis and the prediction of porosity in sandstone and carbonate reservoirs. *AAPG Bulletin*, **96**, 2193–2214, https://doi.org/10.1306/04301211139

Blanchet, C.L., Tjallingii, R., Schleicher, A.M., Schouten, S., Frank, M. and Brauer, A. 2021. Deoxygenation dynamics on the western Nile deep-sea fan during sapropel S1 from seasonal to millennial timescales. *Climate of the Past*, **17**, 1025–1050, https://doi.org/10.5194/CP-17-1025-2021

Bond, D.P.G. and Wignall, P.B. 2010. Pyrite framboid study of marine Permian–Triassic boundary sections: a complex anoxic event and its relationship to contemporaneous mass extinction. *GSA Bulletin*, **122**, 1265–1279, https://doi.org/10.1130/B30042.1

Bontognali, T.R.R., Vasconcelos, C., Warthmann, R.J., Dupraz, C., Bernasconi, S.M. and McKenzie, J.A. 2008. Microbes produce nanobacteria-like structures, avoiding cell entombment. *Geology*, **36**, 663–666, https://doi.org/10.1130/G24755A.1

Böttcher, M.E. and Dietzel, M. 2011. Metal-ion partitioning during low-temperature precipitation and dissolution of anhydrous carbonates and sulphates. *European Mineralogical Union Notes in Mineralogy*, **10**, 139–187, https://doi.org/10.1180/EMU-NOTES.10.4

Bottrell, S. and Raiswell, R. 1989. Primary versus diagenetic origin of Blue Lias rhythms (Dorset, UK): evidence from sulphur geochemistry. *Terra Nova*, **1**, 451–456, https://doi.org/10.1111/J.1365-3121.1989.TB00409.X

Boyd, P.W. and Ellwood, M.J. 2010. The biogeochemical cycle of iron in the ocean. *Nature Geoscience*, **3**, 675–682, https://doi.org/10.1038/NGEO964

Bradbury, H.J., Vandeginste, V. and John, C.M. 2015. Diagenesis of phosphatic hardgrounds in the Monterey Formation: a perspective from bulk and clumped isotope geochemistry. *GSA Bulletin*, **127**, 1453–1463, https://doi.org/10.1130/B31160.1

Brandano, M., Cornacchia, I., Raffi, I., Tomassetti, L. and Jones, B. 2016. The Oligocene–Miocene stratigraphic evolution of the Majella carbonate platform (Central Apennines, Italy). *Sedimentary Geology*, **333**, 1–14, https://doi.org/10.1016/j.sedgeo.2015.12.002

Brenner, S. 2012. Circulation in the Mediterranean Sea. *In*: Stambler, N. (ed.). *Life in the Mediterranean Sea: a Look at Habitat Changes*. Nova Science Publishers, 99–126.

Bridges, T.F., Green, D.I. and Ince, F. 2014. Ankerite: its composition and formulae and its status in the Northern Pennine Orefield. *Journal of the Russell Society*, **17**, 51–56.

Burns, S.J. and Baker, P.A. 1987. A geochemical study of dolomite in the Monterey Formation, California. *Journal of Sedimentary Research*, **57**, 128–139, https://doi.org/10.1306/212F8AC6-2B24-11D7-8648000102C1865D

Casanova-Arenillas, S., Rodríguez-Tovar, F.J. and Martínez-Ruiz, F. 2022. Ichnological evidence for bottom water oxygenation during organic rich layer deposition in the westernmost Mediterranean over the Last Glacial Cycle. *Marine Geology*, **443**, 106673, https://doi.org/10.1016/J.MARGEO.2021.106673

Cipollari, P. and Cosentino, D. 1995. Miocene unconformities in the Central Apennines: geodynamic significance and sedimentary basin evolution. *Tectonophysics*, **252**, 375–389, https://doi.org/10.1016/0040-1951(95)00088-7

Clarkson, M.O., Poulton, S.W., Guilbaud, R. and Wood, R.A. 2014. Assessing the utility of Fe/Al and Fe-speciation to record water column redox conditions in carbonate-rich sediments. *Chemical Geology*, **382**, 111–122, https://doi.org/10.1016/j.chemgeo.2014.05.031

Cornacchia, I., Brandano, M. and Agostini, S. 2021. Miocene paleoceanographic evolution of the Mediterranean area and carbonate production changes: a review. *Earth-Science Reviews*, **221**, 103785, https://doi.org/10.1016/J.EARSCIREV.2021.103785

Cornacchia, I., Brandano, M., Agostini, S. and Munnecke, A. 2022. Neodymium isotopes of central Mediterranean phosphatic hardgrounds reveal Miocene paleoceanography. *Geology*, **50**, 1023–1027, https://doi.org/10.1130/G50118.1

Cramp, A. and O'Sullivan, G. 1999. Neogene sapropels in the Mediterranean: a review. *Marine Geology*, **153**, 11–28, https://doi.org/10.1016/S0025-3227(98)00092-9

Curtis, C.D., Coleman, M.L. and Love, L.G. 1986. Pore water evolution during sediment burial from isotopic and mineral chemistry of calcite, dolomite and siderite concretions. *Geochimica et Cosmochimica Acta*, **50**, 2321–2334, https://doi.org/10.1016/0016-7037(86)90085-2

Dart, C.J., Bosence, D.W.J. and McClay, K.R. 1993. Stratigraphy and structure of the Maltese graben system. *Journal of the Geological Society, London*, **150**, 1153–1166, https://doi.org/10.1144/GSJGS.150.6.1153

de la Vara, A. and Meijer, P. 2016. Response of Mediterranean circulation to Miocene shoaling and closure of the Indian Gateway: a model study. *Palaeogeography, Palaeoclimatology, Palaeoecology*, **442**, 96–109, https://doi.org/10.1016/J.PALAEO.2015.11.002

Dijkstra, N., Kraal, P., Kuypers, M.M.M., Schnetger, B. and Slomp, C.P. 2014. Are iron-phosphate minerals a sink for phosphorus in anoxic Black Sea sediments? *PLoS One*, **9**, e101139, https://doi.org/10.1371/JOURNAL.PONE.0101139

Drake, N.A., Blench, R.M., Armitage, S.J., Bristow, C.S. and White, K.H. 2011. Ancient watercourses and biogeography of the Sahara explain the peopling of the desert. *Proceedings of the National Academy of Sciences of the United States of America*, **108**, 458–462, https://doi.org/10.1073/PNAS.1012231108

Drake, N.A., Candy, I. *et al.* 2022. Sedimentary and geomorphic evidence of Saharan megalakes: a synthesis. *Quaternary Science Reviews*, **276**, 107318, https://doi.org/10.1016/J.QUASCIREV.2021.107318

Eaton, S. and Robertson, A. 1993. The Miocene Pakhna Formation, southern Cyprus and its relationship to the Neogene tectonic evolution of the Eastern Mediterranean. *Sedimentary Geology*, **86**, 273–296, https://doi.org/10.1016/0037-0738(93)90026-2

Eichhub, P. and Boles, J.R. 2000. Focused fluid flow along faults in the Monterey Formation, coastal California. *GSA Bulletin, GeoScienceWorld*, **112**,

1667–1679, https://doi.org/10.1130/0016-7606(2000)112%3c1667:FFFAFI%3e2.0.CO;2
Emerson, D. 2016. The irony of iron – biogenic iron oxides as an iron source to the ocean. *Frontiers in Microbiology*, **6**, 174190, https://doi.org/10.3389/FMICB.2015.01502/BIBTEX
Essid, J., Saidi, R., Ahmed, A.H., Felhi, M., Fattah, N. and Tlili, A. 2019. Characterization, nomenclature and factors controlling the stability of quartz and opal-CT of Burdigalian and Ypresian siliceous rocks from Tunisia. *Journal of African Earth Sciences*, **155**, 151–160, https://doi.org/10.1016/j.jafrearsci.2019.04.018
Filippelli, G.M., Sierro, F.J., Flores, J.A., Vázquez, A., Utrilla, R., Pérez-Folgado, M. and Latimer, J.C. 2003. A sediment–nutrient–oxygen feedback responsible for productivity variations in Late Miocene sapropel sequences of the western Mediterranean. *Palaeogeography, Palaeoclimatology, Palaeoecology*, **190**, 335–348, https://doi.org/10.1016/S0031-0182(02)00613-2
Filippidi, A. and De Lange, G.J. 2019. Eastern Mediterranean deep water formation during sapropel S1: a reconstruction using geochemical records along a bathymetric transect in the Adriatic outflow region. *Paleoceanography and Paleoclimatology*, **34**, 409–429, https://doi.org/10.1029/2018PA003459
Filippidi, A., Triantaphyllou, M.V. and De Lange, G.J. 2016. Eastern-Mediterranean ventilation variability during sapropel S1 formation, evaluated at two sites influenced by deep-water formation from Adriatic and Aegean seas. *Quaternary Science Reviews*, **144**, 95–106, https://doi.org/10.1016/j.quascirev.2016.05.024
Föllmi, K.B., Gertsch, B., Renevey, J.-P., De Kaenel, E. and Stille, P. 2008. Stratigraphy and sedimentology of phosphate-rich sediments in Malta and south-eastern Sicily (latest Oligocene to early Late Miocene). *Sedimentology*, **55**, 1029–1051, https://doi.org/10.1111/j.1365-3091.2007.00935.x
Friedman, I. and O'Neil, J.R. 1977. *Data of Geochemistry Sixth Edition Chapter KK. Compilation of Stable Isotope Fractionation Factors of Geochemical Interest*. United States Government Printing Office, Washington, DC, Geological Survey Professional Papers, **440-KK**.
Frost, B.W. and Franzen, N.C. 1992. Grazing and iron limitation in the control of phytoplankton stock and nutrient concentration: a chemostat analogue of the Pacific equatorial upwelling zone. *Marine Ecology Progress Series*, **83**, 291–303, https://doi.org/10.3354/meps083291
Gradstein, F.M., Ogg, J.G., Schmitz, M.D. and Ogg, G. (eds) 2020. *Geologic Time Scale 2020*. Elsevier, https://doi.org/10.1016/C2020-1-02369-3
Grant, K.M., Grimm, R., Mikolajewicz, U., Marino, G., Ziegler, M. and Rohling, E.J. 2016. The timing of Mediterranean sapropel deposition relative to insolation, sea-level and African monsoon changes. *Quaternary Science Reviews*, **140**, 125–141, https://doi.org/10.1016/J.QUASCIREV.2016.03.026
Haq, B., Gorini, C., Baur, J., Moneron, J. and Rubino, J.L. 2020. Deep Mediterranean's Messinian evaporite giant: how much salt? *Global and Planetary Change*, **184**, 103052, https://doi.org/10.1016/J.GLOPLACHA.2019.103052
Herut, B., Collier, R. and Krom, M.D. 2002. The role of dust in supplying nitrogen and phosphorus to the southeast Mediterranean. *Limnology and Oceanography*, **47**, 870–878, https://doi.org/10.4319/LO.2002.47.3.0870
Higgins, J.A., Blättler, C.L. *et al.* 2018. Mineralogy, early marine diagenesis and the chemistry of shallow-water carbonate sediments. *Geochimica et Cosmochimica Acta*, **220**, 512–534, https://doi.org/10.1016/J.GCA.2017.09.046
Hounslow, M.W., White, H.E. *et al.* 2017. Miocene humid intervals and establishment of drainage networks by 23 Ma in the central Sahara, southern Libya. *Gondwana Research*, **45**, 118–137, https://doi.org/10.1016/J.GR.2016.11.008
Hüneke, H. and Henrich, R. 2011. Pelagic sedimentation in modern and ancient oceans. *Developments in Sedimentology*, **63**, 215–351, https://doi.org/10.1016/B978-0-444-53000-4.00004-4
Hutchins, D.A., Hare, C.E. *et al.* 2002. Phytoplankton iron limitation in the Humboldt current and Peru upwelling. *Limnology and Oceanography*, **47**, 997–1011, https://doi.org/10.4319/LO.2002.47.4.0997
Immenhauser, A. 2022. On the delimitation of the carbonate burial realm. *The Depositional Record*, **8**, 524–574, https://doi.org/10.1002/DEP2.173
Incarbona, A. and Sprovieri, M. 2020. The postglacial isotopic record of intermediate water connects Mediterranean sapropels and organic-rich layers. *Paleoceanography and Paleoclimatology*, **35**, e2020PA004009, https://doi.org/10.1029/2020PA004009
Issacs, C.M. 1982. Influence of rock composition on kinetics of silica phase changes in the Monterey Formation, *Santa Barbara area, California. Geology*, **10**, 304–308, https://doi.org/10.1130/0091-7613(1982)10<304:IORCOK>2.0.CO;2
Jacobs, E., Weissert, H., Shields, G. and Stille, P. 1996. The Monterey event in the Mediterranean: a record from shelf sediments of Malta. *Paleoceanography*, **11**, 717–728, https://doi.org/10.1029/96PA02230
Jiang, H.B., Hutchins, D.A. *et al.* 2023. Natural ocean iron fertilization and climate variability over geological periods. *Global Change Biology*, **29**, 6856–6866, https://doi.org/10.1111/GCB.16990
Jickells, T. and Moore, C.M. 2015. The importance of atmospheric deposition for ocean productivity. *Annual Review of Ecology, Evolution, and Systematics*, **46**, 481–501, https://doi.org/10.1146/annurev-ecolsys-112414-054118
John, C.M., Mutti, M. and Adatte, T. 2003. Mixed carbonate–siliciclastic record on the North African margin (Malta) – coupling of weathering processes and mid Miocene climate. *GSA Bulletin*, **115**, 217–229, https://doi.org/10.1130/0016-7606(2003)115<0217:MCSROT>2.0.CO;2
Karpoff, A.M., Destrigneville, C. and Stille, P. 2007. Clinoptilolite as a new proxy of enhanced biogenic silica productivity in lower Miocene carbonate sediments of the Bahamas platform: isotopic and thermodynamic evidence. *Chemical Geology*, **245**, 285–304, https://doi.org/10.1016/J.CHEMGEO.2007.08.011
Kidd, R.B. and Ryan, W.B.F. 1978. Stratigraphy of Eastern Mediterranean sapropel sequences recovered during DSDP Leg 42a and their paleoenvironmental significance. *Initial Reports of the Deep Sea Drilling Project*, **42**, https://doi.org/10.2973/DSDP.PROC.42-1.113-1.1978
Kocken, I.J., Cramwinckel, M.J., Zeebe, R.E., Middelburg, V.J. and Sluijs, A. 2019. The 405 kyr and 2.4 Myr eccentricity components in Cenozoic carbon isotope records. *Climate of the Past*, **15**, 91–104, https://doi.org/10.5194/CP-15-91-2019
Laskar, J., Robutel, P., Joutel, F., Gastineau, M., Correia, A.C.M. and Levrard, B. 2004. A long-term numerical solution for the insolation quantities of the Earth. *Astronomy and Astrophysics*, **428**, 261–285, https://doi.org/10.1051/0004-6361:20041335
Leonova, G.A., Maltsev, A.E., Melenevsky, V.N., Krivonogov, S.K., Kondratyeva, L.M., Bobrov, V.A. and Suslova, M.Y. 2019. Diagenetic transformation of organic matter in sapropel sediments of small lakes (southern West Siberia and eastern Transbaikalia). *Quaternary International*, **524**, 40–47, https://doi.org/10.1016/J.QUAINT.2019.03.011
Li, C., Dong, L., Ma, H., Liu, H., Li, C., Pei, H. and Shen, B. 2022. Formation of the massive bedded chert and coupled silicon and iron cycles during the Ediacaran–Cambrian transition. *Earth and Planetary Science Letters*, **594**, 117721, https://doi.org/10.1016/J.EPSL.2022.117721
Liu, D., Cao, J., *et al.* 2024. Microbially-mediated formation of Ca–Fe carbonates during dissimilatory ferrihydrite reduction: implications for the origin of sedimentary ankerite. *Science China Earth Sciences*, **67**, 208–221, https://doi.org/10.1007/s11430-022-1164-2
Lyu, J., Auer, G., Bialik, O.M., Christensen, B., Yamaoka, R. and De Vleeschouwer, D. 2023. Astronomically-paced changes in paleoproductivity, winnowing and mineral flux over Broken Ridge (Indian Ocean) since the Early Miocene. *Paleoceanography and Paleoclimatology*, **38**, e2023PA004761, https://doi.org/10.1029/2023PA004761
Madsen, H.B. and Stemmerik, L. 2010. Diagenesis of flint and porcellanite in the Maastrichtian Chalk at Stevns Klint, Denmark. *Journal of Sedimentary Research*, **80**, 578–588, https://doi.org/10.2110/jsr.2010.052
Maliva, R.G. and Siever, R. 1989. Nodular chert formation in carbonate rocks. *The Journal of Geology*, **97**, 421–433, http://www.jstor.org/stable/30078348
Maliva, R.G., Knoll, A.H. and Simonson, B.M. 2005. Secular change in the Precambrian silica cycle: insights from chert petrology. *GSA Bulletin*, **117**, 835–845, https://doi.org/10.1130/B25555.1
Mancini, A.M., Bocci, G., Morigi, C., Gennari, R., Lozar, F. and Negri, A. 2023. Past analogues of deoxygenation events in the Mediterranean Sea: a tool to constrain future impacts. *Journal of Marine Science and Engineering*, **11**, 562, https://doi.org/10.3390/JMSE11030562/S1
Martin, J.H. 1990. Glacial–interglacial CO_2 change: the iron hypothesis. *Paleoceanography*, **5**, 1–13, https://doi.org/10.1029/PA005I001P00001
McCrea, J.M. 1950. On the isotopic chemistry of carbonates and a paleotemperature scale. *The Journal of Chemical Physics*, **18**, 849–857, https://doi.org/10.1063/1.1747785
Meijer, P. 2021. (Paleo)oceanography of semi-enclosed seas with a focus on the Mediterranean region; insights from basic theory. *Earth-Science Reviews*, **221**, 103810, https://doi.org/10.1016/J.EARSCIREV.2021.103810
Meister, P., Herda, G., Petrishcheva, E., Gier, S., Dickens, G.R., Bauer, C. and Liu, B. 2022. Microbial alkalinity production and silicate alteration in methane charged marine sediments: implications for porewater chemistry and diagenetic carbonate formation. *Frontiers in Earth Science*, **9**, 756591, https://doi.org/10.3389/FEART.2021.756591/BIBTEX
Meyer, K.M. and Kump, L.R. 2008. Oceanic euxinia in Earth history: causes and consequences. *Annual Review of Earth and Planetary Sciences*, **36**, 251–288, https://doi.org/10.1146/annurev.earth.36.031207.124256
Miller, K.G., Browning, J.V., Schmelz, W.J., Kopp, R.E., Mountain, G.S. and Wright, J.D. 2020. Cenozoic sea-level and cryospheric evolution from deep-sea geochemical and continental margin records. *Science Advances*, **6**, eaaz1346, https://doi.org/10.1126/sciadv.aaz1346
Mourik, A.A., Abels, H.A., Hilgen, F.J., Di Stefano, A. and Zachariasse, W.J. 2011. Improved astronomical age constraints for the middle Miocene climate transition based on high-resolution stable isotope records from the central Mediterranean Maltese Islands. *Paleoceanography*, **26**, https://doi.org/10.1029/2010PA001981
Ohfuji, H. and Rickard, D. 2005. Experimental syntheses of framboids – a review. *Earth-Science Reviews*, **71**, 147–170, https://doi.org/10.1016/J.EARSCIREV.2005.02.001
Oren, O.H. 1969. Oceanographic and biological influence of the Suez Canal, the Nile and the Aswan Dam on the Levant Basin. *Progress in Oceanography*, **5**, 161–167, https://doi.org/10.1016/0079-6611(69)90038-X
Oretade, B.S. 2021. Calcareous nannofloras in Western Lobe Offshore, Niger Delta: eutrophication and climate change implications. *Geografia: Malaysian Journal of Society and Space*, **17**, 274–287, https://doi.org/10.17576/geo-2021-1704-19
Passier, H.F. and De Lange, G.J. 1998. Sedimentary sulfur and iron chemistry in relation to the formation of eastern Mediterranean sapropels. *Proceedings of the Ocean Drilling Program: Scientific Results*, **160**, 249–260, https://doi.org/10.2973/ODP.PROC.SR.160.020.1998

Pedley, M. 1996. Miocene reef facies of the Pelagian region (Central Mediterranean). *SEPM Concepts in Sedimentology and Paleontology*, **5**, https://doi.org/10.2110/csp.96.05

Pedley, H.M., House, M.R. and Waugh, B. 1978. The geology of the Pelagian Block: the Maltese Islands. *In*: Nairn, A.E.M., Kanes, W.H. and Stehli, F.G. (eds) *The Ocean Basins and Margins*. Springer, 417–433, https://doi.org/10.1007/978-1-4684-3039-4_8

Pérez-Asensio, J.N., Frigola, J. *et al.* 2020. Changes in western Mediterranean thermohaline circulation in association with a deglacial organic rich layer formation in the Alboran Sea. *Quaternary Science Reviews*, **228**, 106075, https://doi.org/10.1016/J.QUASCIREV.2019.106075

Petrash, D.A., Robbins, L.J., Shapiro, R.S., Mojzsis, S.J. and Konhauser, K.O. 2016. Chemical and textural overprinting of ancient stromatolites: timing, processes and implications for their use as paleoenvironmental proxies. *Precambrian Research*, **278**, 145–160, https://doi.org/10.1016/J.PRECAMRES.2016.03.010

Petrash, D.A., Bialik, O.M., Bontognali, T.R.R., Vasconcelos, C., Roberts, J.A., McKenzie, J.A. and Konhauser, K.O. 2017. Microbially catalyzed dolomite formation: from near-surface to burial. *Earth-Science Reviews*, **171**, 558–582, https://doi.org/10.1016/J.EARSCIREV.2017.06.015

Petrash, D.A., Bialik, O.M., Staudigel, P.T., Konhauser, K.O. and Budd, D.A. 2021. Biogeochemical reappraisal of the freshwater–seawater mixing-zone diagenetic model. *Sedimentology*, **68**, 1797–1830, https://doi.org/10.1111/SED.12849

Petrash, D.A., Steenbergen, I.M., Valero, A., Meador, T.B., Paces, T. and Thomazo, C. 2022. Aqueous system-level processes and prokaryote assemblages in the ferruginous and sulfate-rich bottom waters of a post-mining lake. *Biogeosciences*, **19**, 1723–1751, https://doi.org/10.5194/BG-19-1723-2022

Poulton, S.W. and Canfield, D.E. 2005. Development of a sequential extraction procedure for iron: implications for iron partitioning in continentally derived particulates. *Chemical Geology*, **214**, 209–221, https://doi.org/10.1016/J.CHEMGEO.2004.09.003

Raiswell, R. and Canfield, D.E. 1998. Sources of iron for pyrite formation in marine sediments. *American Journal of Science*, **298**, 219–245, https://doi.org/10.2475/AJS.298.3.219

Reich, T., Ben-Ezra, T. *et al.* 2022. A year in the life of the Eastern Mediterranean: monthly dynamics of phytoplankton and bacterioplankton in an ultra-oligotrophic sea. *Deep Sea Research Part I: Oceanographic Research Papers*, **182**, 103720, https://doi.org/10.1016/J.DSR.2022.103720

Riahi, S., Soussi, M. and Ben-Ismail-Lattrache, K. 2015. Age, internal stratigraphic architecture and structural style of the Oligocene–Miocene Numidian Formation of northern Tunisia. *Annales Societatis Geologorum Poloniae*, **85**, 345–370, https://doi.org/10.14241/ASGP.2015.009

Rickard, D. 2019. Sedimentary pyrite framboid size-frequency distributions: a meta-analysis. *Palaeogeography, Palaeoclimatology, Palaeoecology*, **522**, 62–75, https://doi.org/10.1016/j.palaeo.2019.03.010

Rögl, F. 1999. Mediterranean and Paratethys. Facts and hypotheses of an Oligocene to Miocene paleogeography (short overview). *Geologica Carpathica*, **50-4**, 339–349.

Rohling, E.J. 1994. Review and new aspects concerning the formation of eastern Mediterranean sapropels. *Marine Geology*, **122**, 1–28, https://doi.org/10.1016/0025-3227(94)90202-X

Rohling, E.J., Marino, G. and Grant, K.M. 2015. Mediterranean climate and oceanography and the periodic development of anoxic events (sapropels). *Earth-Science Reviews*, **143**, 62–97, https://doi.org/10.1016/J.EARSCIREV.2015.01.008

Rosenbaum, J. and Sheppard, S.M.F. 1986. An isotopic study of siderites, dolomites and ankerites at high temperatures. *Geochimica et Cosmochimica Acta*, **50**, 1147–1150, https://doi.org/10.1016/0016-7037(86)90396-0

Roveri, M., Lugli, S., Manzi, V., Reghizzi, M. and Rossi, F.P. 2020. Stratigraphic relationships between shallow-water carbonates and primary gypsum: insights from the Messinian succession of the Sorbas Basin (Betic Cordillera, southern Spain). *Sedimentary Geology*, **404**, 105678, https://doi.org/10.1016/J.SEDGEO.2020.105678

Rubin-Blum, M., Antler, G. *et al.* 2014. Hydrocarbon-related microbial processes in the deep sediments of the Eastern Mediterranean Levantine Basin. *FEMS Microbiology Ecology*, **87**, 780–796, https://doi.org/10.1111/1574-6941.12264

Rutten, A., De Lange, G.J., Hayes, A., Rohling, E.J., De Jong, A.F.M. and Van Der Borg, K. 1999. Deposition of sapropel S1 sediments in oxic pelagic and anoxic brine environments in the eastern Mediterranean: differences in diagenesis and preservation. *Marine Geology*, **153**, 319–335, https://doi.org/10.1016/S0025-3227(98)00076-0

Sela-Adler, M., Herut, B. *et al.* 2015. Geochemical evidence for biogenic methane production and consumption in the shallow sediments of the SE Mediterranean shelf (Israel). *Continental Shelf Research*, **101**, 117–124, https://doi.org/10.1016/J.CSR.2015.04.001

Sibert, E.C. and Rubin, L.D. 2021. An early Miocene extinction in pelagic sharks. *Science*, **372**, 1105–1107, https://doi.org/10.1126/SCIENCE.AAZ3549/

Sigl, W., Chamley, H., Fabricus, F., Giroud d'Argoud, G. and Muller, J. 1978. Sedimentology and environmental conditions of sapropels. *Deep Sea Drilling Project Initial Reports*, **42**, part 1, section 13.1, https://doi.org/10.2973/dsdp.proc.42-1.113-2.1978

Sinninghe Damst'e, J.S., Rijpstra, W.I.C., Kock-van Dalen, A.C., De Leeuw, J.W. and Schenck, P.A. 1989. Quenching of labile functionalised lipids by inorganic sulphur species: evidence for the formation of sedimentary organic sulphur compounds at the early stages of diagenesis. *Geochimica et Cosmochimica Acta*, **53**, 1343–1355, https://doi.org/10.1016/0016-7037(89)90067-7

Sisma-Ventura, G., Bialik, O.M. *et al.* 2022. Cold seeps alter the near-bottom biogeochemistry in the ultraoligotrophic southeastern Mediterranean Sea. *Deep Sea Research Part I: Oceanographic Research Papers*, **183**, 103744, https://doi.org/10.1016/J.DSR.2022.103744

Taylforth, J.E., McCay, G.A., Ellam, R., Raffi, I., Kroon, D. and Robertson, A.H.F. 2014. Middle Miocene (Langhian) sapropel formation in the easternmost Mediterranean deep-water basin: evidence from northern Cyprus. *Marine and Petroleum Geology*, **57**, 521–536, https://doi.org/10.1016/J.MARPETGEO.2014.04.015

Thomson, J., Crudeli, D., De Lange, G.J., Slomp, C.P., Erba, E., Corselli, C. and Calvert, S.E. 2004. *Florisphaera profunda* and the origin and diagenesis of carbonate phases in eastern Mediterranean sapropel units. *Paleoceanography*, **19**, https://doi.org/10.1029/2003PA000976

Urban, N.R., Ernst, K. and Bernasconi, S. 1999. Addition of sulfur to organic matter during early diagenesis of lake sediments. *Geochimica et Cosmochimica Acta*, **63**, 837–853, https://doi.org/10.1016/S0016-7037(98)00306-8

Watson, A.J., Bakker, D.C.E., Ridgwell, A.J., Boyd, P.W. and Law, C.S. 2000. Effect of iron supply on Southern Ocean CO_2 uptake and implications for glacial atmospheric CO_2. *Nature*, **407**, 730–733, https://doi.org/10.1038/35037561

Westerhold, T., Marwan, N. *et al.* 2020. An astronomically dated record of Earth's climate and its predictability over the last 66 million years. *Science*, **369**, 1383–1388, https://doi.org/10.1126/SCIENCE.ABA6853

Wignall, P.B. and Newton, R. 1998. Pyrite framboid diameter as a measure of oxygen deficiency in ancient mudrocks. *American Journal of Science*, **298**, 537–552, https://doi.org/10.2475/ajs.298.7.537

Wilkin, R.T., Barnes, H.L. and Brantley, S.L. 1996. The size distribution of framboidal pyrite in modern sediments: an indicator of redox conditions. *Geochimica et Cosmochimica Acta*, **60**, 3897–3912, https://doi.org/10.1016/0016-7037(96)00209-8

Wilkin, R.T., Arthur, M.A. and Dean, W.E. 1997. History of water-column anoxia in the Black Sea indicated by pyrite framboid size distributions. *Earth and Planetary Science Letters*, **148**, 517–525, https://doi.org/10.1016/S0012-821X(97)00053-8

Woods, T.L. and Garrels, R.M. 1992. Calculated aqueous-solution-solid-solution relations in the low-temperature system CaO–MgO–FeO–CO_2–H_2O. *Geochimica et Cosmochimica Acta*, **56**, 3031–3043, https://doi.org/10.1016/0016-7037(92)90288-T

Wu, C.H., Lee, S.Y. and Tsai, P.C. 2021. Role of eccentricity in early Holocene African and Asian summer monsoons. *Scientific Reports*, **11**, 1–13, https://doi.org/10.1038/s41598-021-03525-z

Wurgaft, E., Findlay, A.J., Vigderovich, H., Herut, B. and Sivan, O. 2019. Sulfate reduction rates in the sediments of the Mediterranean continental shelf inferred from combined dissolved inorganic carbon and total alkalinity profiles. *Marine Chemistry*, **211**, 64–74, https://doi.org/10.1016/J.MARCHEM.2019.03.004

Zammit, R., Lear, C.H., Samankassou, E., Lourens, L.J., Micallef, A., Pearson, P.N. and Bialik, O.M. 2022. Early Miocene intensification of the North African hydrological cycle: multi-proxy evidence from the shelf carbonates of Malta. *Paleoceanography and Paleoclimatology*, **37**, e2022PA004414, https://doi.org/10.1029/2022PA004414

Zirks, E., Krom, M.D., Zhu, D., Schmiedl, G. and Goodman-Tchernov, B.N. 2019. Evidence for the presence of oxygen-depleted sapropel intermediate water across the Eastern Mediterranean during Sapropel S1. *ACS Earth and Space Chemistry*, **3**, 2287–2297, https://doi.org/10.1021/acsearthspacechem.9b00128